RESEARCH REPORT

Institute of Transportation Studies | UNIVERSITY OF CALIFORNIA

Evaluating the Seismic Vulnerability and Resilience of BART's Berkeley Hills Tunnel

Esra Zengin, Ph.D., Postdoctoral Scholar, UCLA
Yousef Bozorgnia, Ph.D., P.E., Professor, Civil and Environmental Engineering, UCLA
Jonathan P. Stewart, Ph.D., P.E., Professor, Civil and Environmental Engineering, UCLA

January 2025

California Resilient and Innovative Mobility Initiative

Report No.: UC-ITS-2024-48-4V | DOI: 10.7922/G22J697K

Technical Report Documentation Page

1. Report No. UC-ITS-2024-48-4V	**2. Government Accession No.** N/A	**3. Recipient's Catalog No.** N/A
4. Title and Subtitle Evaluating the Seismic Vulnerability and Resilience of BART's Berkeley Hills Tunnel		**5. Report Date** January 2025 **6. Performing Organization Code** UCLA-ITS
7. Author(s) Esra Zengin, Ph.D., https://orcid.org/0000-0002-6543-4526; Yousef Bozorgnia, Ph.D., P.E., https://orcid.org/0000-0003-1773-2489; Jonathan P. Stewart, Ph.D., P.E., https://orcid.org/0000-0003-3602-3629		**8. Performing Organization Report No.** N/A
9. Performing Organization Name and Address Institute of Transportation Studies, UCLA 3320 Public Affairs Building Los Angeles, CA 90095-1656		**10. Work Unit No.** N/A **11. Contract or Grant No.** UC-ITS-2024-48-4V
12. Sponsoring Agency Name and Address The University of California Institute of Transportation Studies www.ucits.org		**13. Type of Report and Period Covered** Final Report (September 2023-September 2024) **14. Sponsoring Agency Code** UC ITS
15. Supplementary Notes DOI: 10.7922/G22J697K		

16. Abstract

Critical nodes in transportation networks, such as major transit tunnels and interchange stations, are vital for maintaining system functionality following a disruptive event such as a large earthquake. This project focuses on evaluating the seismic resilience of BART's Berkeley Hills Tunnel that intersects the Hayward Fault, one of California's most active seismic zones. The Hayward Fault poses a significant risk, with the potential for a magnitude 7+ earthquake that could severely impact the tunnel, potentially disrupting BART service and affecting the broader transit network. This study employs the latest fault displacement hazard data and models to estimate the probability of fault rupture displacements and assesses the resulting damage. It then evaluates the likelihood of service interruptions caused by potential Hayward Fault events. The results suggest that the tunnels may experience minor to significant damage depending on the amplitude of the fault displacement, which can lead to repair times ranging from a few weeks to over a year. The findings highlight the importance of improving tunnel resilience to minimize service disruptions and ensure efficient recovery following major earthquakes.

17. Key Words Earthquakes, rail transit facilities, tunnels, finite element method, computer models, disaster resilience, earthquake engineering		**18. Distribution Statement** No restrictions.	
19. Security Classification (of this report) Unclassified	**20. Security Classification (of this page)** Unclassified	**21. No. of Pages** 53	**22. Price** N/A

Form Dot F 1700.7 (8-72) Reproduction of completed page authorized

About the UC Institute of Transportation Studies

The University of California Institute of Transportation Studies (UC ITS) is a network of faculty, research and administrative staff, and students dedicated to advancing the state of the art in transportation engineering, planning, and policy for the people of California. Established by the Legislature in 1947, ITS has branches at UC Berkeley, UC Davis, UC Irvine, and UCLA.

Acknowledgments

This study was made possible with funding received by the University of California Institute of Transportation Studies from the State of California through the Road Repair and Accountability Act of 2017 (Senate Bill 1) Initiative. The authors would like to thank the State of California for its support of university-based research, and especially for the funding received for this project. The authors would also like to thank Professor Kenichi Soga of UC Berkeley, Professor Louise Comfort of the University of Pittsburg, and Graduate Student Tianyu Han of UC Berkeley for their collaboration and Andrew Shuck of BART for engaging in fruitful technical discussions. Additionally, special thanks to Steve Thompson, Arash Zandieh, Alex Sarmiento for providing fault displacement data for the BART tunnel crossing the Hayward Fault. This work used computational and storage services associated with the Hoffman2 Cluster which is operated by the UCLA Office of Advanced Research Computing's Research Technology Group.

Disclaimer

Institute of Transportation Studies | UNIVERSITY OF CALIFORNIA

Evaluating the Seismic Vulnerability and Resilience of BART's Berkeley Hills Tunnel

Esra Zengin, Ph.D., Postdoctoral Scholar, UCLA
Yousef Bozorgnia, Ph.D., P.E., Professor, Civil and Environmental Engineering, UCLA
Jonathan P. Stewart, Ph.D., P.E., Professor, Civil and Environmental Engineering, UCLA

January 2025

California Resilient and Innovative Mobility Initiative

Report No.: UC-ITS-2024-48-4V | DOI: 10.7922/G22J697K

Table of Contents

Table of Contents

Executive Summary **1**
Introduction **4**
Background 4
Objectives and Scope 5
Organization of Report 6
Three-Dimensional Finite Element Model of the BART Berkeley Hills Tunnel **7**
BART System Overview and Vulnerability 7
BART Berkeley Hills Tunnel 11
Tunnel Computer Modeling Approach 14
Assessing Tunnel Structural Damage Under Fault Displacement and BART System Resilience **22**
Probabilistic Fault Displacement Hazard Analysis 22
Deformation Characteristics 24
Tunnel Lining Stresses 27
Quantification of the Tunnel Damage 29
Functionality Impact and Restoration Timeline 32
Conclusions **35**
References **37**

List of Tables

Table 1. Mechanical properties of the surrounding rock. 16

Table 2. CDP plasticity parameters 17

Table 3. Structural Damage Characteristics, Functionality Impact, and Restoration Timelines for Tunnel Lining at Various Fault Displacement Levels, Along with Associated Return Periods and Exceedance Probabilities. 33

List of Figures

Figure 1. BART system map (left panel), and the Bay Area faults in the BART service area (right panel) (https://www.bart.gov/about/projects/eqs) 8

Figure 2. Seismic Performance Objectives for BART Retrofit Program (City and County of San Francisco 2020). 11

Figure 3. Cross section of the Berkeley Hills Tunnel (from Brown et al. 1981). 12

Figure 4. Geological formation along the BART tunnel through Berkeley Hills (after Bechtel 1968). 13

Figure 5. a) Section of tunnel in Hayward Fault zone, surrounding rocks and location of instrumentation, b) Liner crack pattern for 10 years (1969-1979) of creep displacement (Brown et al. 1981). 14

Figure 6. a) 3D ABAQUS finite element model of the tunnel b) tunnel cross-section, highlighting the crown at the top, the invert at the bottom, and the left and right walls. 16

Figure 7. Uniaxial compression (left panel) and tension (right panel) stress-strain curves of CDP (Dassault Systèmes Simulia Corp., 2016) 19

Figure 8.a) Compression and b) tension stress-strain relationships and damage factors for C20 concrete adopted in the model. 19

Figure 9. Comparisons of the crack patterns observed in BART tunnel with the simulated tensile cracking patterns of the concrete tunnel liner under a 10-year creep displacement of 0.04 m. 21

Figure 10. Fault displacement hazard curves from LA23 and KEA24 models (Courtesy: Thompson, Zandieh, Sarmiento, 2024) 23

Figure 11. a) Horizontal displacement profiles of the right wall of the tunnel and the free-field rock for a fault displacement of 1.5 m, b) Displacement gradients under various fault displacement levels. 24

Figure 12. Longitudinal strain distributions along the tunnel axis at various fault displacement levels: a) crown, b) invert, c) left wall, d) right wall of the tunnel. Positive in tension, negative in compression. 25

Figure 13. Curvature profile along the tunnel axis. 26

Figure 14. Figure 14. Shear strain distributions along the tunnel axis at various fault displacement levels: a) crown, b) invert. (units in decimal format) 27

Figure 15. a) Maximum principal stress, b) Minimum principal stress, and c) Shear stress distributions of the tunnel lining, d) Von Misses stress distributions in the reinforcement steel bars for a fault displacement of 1.5 m (units in Pascal). 28

Figure 16. a) The maximum Von Mises stresses at the crown, invert, and right and left walls of the tunnel for various $Egouge/Eserp$ ratios b) The impact of fault zone cohesion on lining stresses. 29

Figure 17. Strain vs. Compression/Tension damage, shear strain capacity of the C20, and the steel yielding strain. 30

Figure 18. a) Concrete tension damage (DAMAGET) distributions along the tunnel axis at fault displacements of a) 0.04 m and b) 0.2 m, corresponding to the 10-year and 60-year creep displacements c) Concrete compression damage (DAMAGEC) and d) DAMAGET distributions along the tunnel axis at a fault displacement of 1.5 m. 31

Executive Summary

Executive Summary

A strong earthquake can cause the ground to shift up to several meters on either side of the fault line, known as fault displacement. This poses a major challenge to tunnels passing through fault zones. Understanding the impact an earthquake can have on a tunnel is essential for analyzing the potential risk to the overall transportation system and planning for the effects of post-event service disruptions. The Hayward Fault in the San Francisco Bay Area poses a significant risk of magnitude 7+ earthquakes, which would seriously damage the Berkeley Hills Tunnel, disrupting service for the Bay Area Rapid Transit (BART) system and affecting the wider transit network in the region. This study uses recently developed advanced fault displacement hazard data and models to estimate the likelihood of such an event, evaluates the damage caused by ground displacements on BART's tunnel liner systems and the potential for service interruptions from that damage, and estimates the time needed for repairs based on the severity of the damage.

We utilized an advanced computer simulation approach to develop a three-dimensional model of this dual bore tunnel system and the surrounding rock materials. The computer model was then validated by comparing the simulation results with observed crack patterns in the tunnel lining from long-term fault movements, known as creep displacement, which were in good agreement. We then performed simulations for larger levels of fault displacement associated with longer periods of creep and with earthquakes of different sizes. The results showed that both of the tunnels can experience minor to severe damage depending on the amplitude of the ground displacement from a fault rupture, with stresses and strains concentrating near the fault plane. We predict that service disruptions from minor displacements that can be anticipated over the next 50 years (0.2 m based on current creep rate estimates) would be manageable. However, we also predict that there is a 10 percent chance of a 1.0 m fault displacement taking place from a 500-year earthquake within the 50-year lifespan of the tunnel which would result in significant damage to the tunnel and prolonged tunnel closure. Repair times may range from approximately one to four weeks for minor displacements (from creep) to 12-24 months for severe cases (the 500-year earthquake).

These results suggest that the tunnel does not achieve BART system's long-term performance goal of remaining operational during a 500-year seismic event. This highlights the necessity for ongoing monitoring and proactive measures to mitigate damage and disruption to transit operations.

The Local Hazard Mitigation Plan (2017) proposed designing a bypass for the Berkeley Hills Tunnel as part of its mitigation strategy, suggesting the creation of an alternate route around a vulnerable section of the tunnel. However, this action was assigned a lower priority compared to other initiatives in the 2022 update of the plan (Local Hazard Mitigation Plan 2022). Another potential mitigation strategy may involve retrofitting the existing tunnel by adjusting its geometry such as enlarging the tunnel diameter and increasing the liner thickness to facilitate relatively rapid repair following fault displacement. However, this study did not evaluate how such modifications would impact tunnel performance under fault displacement. Thus, further studies are needed to examine the feasibility and effectiveness of these retrofits.

By understanding the potential impact of fault displacements and preparing for various earthquake scenarios, stakeholders can develop strategic upgrades and robust repair strategies to safeguard tunnel systems, ensure operational continuity, and mitigate economic disruptions. Overall, the insights from this study underscore the need for proactive measures to improve the resilience of tunnels crossing active faults, to prepare for necessary post-event repairs, and to develop strategies for re-routing affected transit service.

Contents

Introduction

Background

As urban centers around the world expand and densify, many transportation networks are becoming increasingly reliant on underground tunnels and stations. In seismically active regions like the western United States Turkey, China, and Japan, this reliance introduces significant challenges due to the potential vulnerability of tunnels to seismic hazards. Seismic impacts on tunnels generally fall into two categories: ground shaking and ground failure. Ground shaking, caused by seismic waves propagating through the Earth, results in vibrations that can affect tunnels, but experience suggests these impacts are generally modest (Gao et al. 2024). Ground failure, including phenomena like liquefaction, slope instability, and fault rupture, produces permanent ground displacement; such displacements pose the most direct threat to tunnels (e.g., Pitilakis and Tsinidis 2013). This research focuses on hazards associated with ground displacement across a fault zone during an earthquake, known as *fault displacement*, which entails a sudden shift along a fault during an earthquake, causing ground cracks and potential damage to structures. Earthquakes are not the only source of fault movements, which can also result from the slower, ongoing movement of earth along faults lines—known as *creep-induced displacement*—that can gradually degrade tunnel structures over time (McGarr and Fletcher 2003, Leone et al. 2024). Addressing both types of displacement is crucial for ensuring the resilience and safety of tunnels in seismic regions.

Historical seismic events illustrate the severe impact of fault displacements on mountain and underground tunnels. For example, the 1906 San Francisco earthquake caused significant damage to tunnels crossing the San Andreas Fault (Thatcher et al. 1997). The 1995 Hyogo-ken Nanbu earthquake near Kobe, Japan, caused extensive damage to numerous tunnels (Asakura and Sato 1998, Iida et al. 1996, Uenishi and Sakurai 2000). The 1999 Chi-Chi earthquake in Taiwan and the 1999 Duzce earthquake in Turkey similarly resulted in considerable tunnel damage and collapses (Hashash et al. 2001, Wang et al. 2001, Ulusay et al. 2002). The 2008 Wenchuan earthquake in China severely affected the Longxi Tunnel (Yu et al. 2016, Lai et al. 2017). These historical events underscored the vulnerability of tunnels to various types of damage caused by fault displacements, including shear and bending cracks and failures, concrete lining spalling, localized buckling, groundwater inflow, and even total collapse (Owen and Scholl 1981, Anastasopoulos et al. 2008). To reduce these risks, several strategies have been developed, such as the use of flexible joints, reinforcing tunnel linings with stronger materials, implementing and improving ground stabilization around the tunnel (Russo et al. 2002).

Recent studies have advanced our understanding of tunnel damage mechanisms in fault zones through experimental, analytical, and numerical approaches. Experimental research, though less common due to challenges in scaling relationships (i.e., replicating in situ stress conditions), provides valuable validation for numerical and analytical models. Many researchers have conducted scale model tests and centrifuge tests to observe tunnel behavior under various fault mechanisms (Burridge et al. 1989, Tsinidis et al. 2015). Analytical models provide frameworks for understanding tunnel behavior under fault displacements, with foundational work by Newmark (1975) and Kennedy et al. (1977) focusing on axial deformations in soil-structure interaction

constrained by frictional forces. Advanced solutions in the literature include models to predict lining forces and deformations for tunnel design (Zhao et al. 2017), assess seismic responses of fault-crossing tunnels with multiple flexible joints (Yan et al. 2022), evaluate pipeline or tunnel behavior under reverse fault movement, where one block moves upward relative to the other due to compressive forces (Tao et al. 2023), and account for fault zone width and nonlinear tunnel-soil interaction (Zhang et al. 2024). Numerical modeling is a powerful tool for predicting tunnel behavior during earthquakes. Methods such as beam-spring models (Hashash et al. 2001), the finite element method (FEM) and the finite difference method (FDM) have been extensively used (Lanzano et al. 2008, Corigliano et al. 2011, Luo and Yang 2013, Ma et al. 2019, Zhen et al. 2022, Wang and Geng 2024). These studies provided insights into how factors like the fault's intersection angle, fault zone width, segment length, section shape, and material properties affect the distribution of stresses acting on tunnel liners and the resulting damage.

One of the lessons from prior studies is that the impacts of fault ruptures on tunnels depend on particular details of the fault, its angle with respect to the tunnel, the type of fault movement, and structural details related to the tunnel liner. As a result, to reliably assess the impacts of fault rupture hazards, studies specific to the conditions of a particular tunnel and fault are essential. This research conducts such an investigation for the Bay Area Rapid Transit (BART) Berkeley Hills Tunnel crossing the Hayward Fault, a major seismic fault in the San Francisco Bay Area, where fault displacement threatens both the structural integrity and operational continuity of this important transportation corridor. Considering the Hayward Fault's high risk of future earthquakes, it is essential to understand the impact of fault displacement on this tunnel to facilitate planning for disaster response including establishing alternate transportation routes and marshalling resources needed for tunnel repair. The overall aim is to minimize disruption to the BART system, which is a crucial transportation link for the San Francisco Bay Area.

Objectives and Scope

To evaluate the seismic vulnerability and risk of BART's Berkeley Hills Tunnel we constructed a nonlinear FEM model and validated it by comparing the results to observed crack patterns in the tunnel lining caused by the slow, gradual movement of the active Hayward Fault, known as creep-induced displacement. The study utilizes the latest findings and models of the Fault Displacement Hazard Initiative (FDHI), a multi-year, community-based research project of the University of California for updating the state-of-practice in fault displacement hazard analysis. The FDHI developed database, models and tools to estimate the annual probability of a ground displacement across a fault that exceeds a certain level. We apply those tools in this project and quantify the resulting damage to the tunnel lining. The findings offer critical insights for managing seismic risk, protecting tunnel functions and estimating the time needed for repairs to restore service.

Organization of Report

The *Introductio*n highlights research on tunnel damage and the importance of identifying fault displacement hazards for tunnels crossing earthquake faults. The section titled *Three-Dimensional Finite Element Model of the BART Berkeley Hills Tunnel* details vulnerabilities, past mitigation efforts, and the development of a FEM model for simulating tunnel behavior under fault displacement. *Assessing Tunnel Structural Damage under Fault Displacement and BART System Resilience* analyzes tunnel deformation and strain distribution, evaluates concrete damage parameters, and uses FDHI models to link displacement exceedance probabilities with functionality and restoration timelines. *Conclusions* summarize findings, implications for seismic risk management, and future research recommendations.

Three-Dimensional Finite Element Model of the BART Berkeley Hills Tunnel

This chapter discusses the seismic vulnerabilities of the Berkeley Hills Tunnel, a crucial component of the Bay Area Rapid Transit (BART) system, which crosses the Hayward Fault near its western portal. It reviews past efforts by BART to improve system resilience against severe earthquakes and highlights the seismic risks associated with the Berkeley Hills Tunnel, emphasizing its strategic importance to the transit network. It also provides information on the geological formations along the tunnel and discusses creep-induced cracking patterns observed in the tunnel lining. Additionally, the chapter details the development and validation of the FEM model used to simulate how the tunnel responds to fault displacement.

BART System Overview and Vulnerability

The BART system, operational since 1972, is a heavy-rail transit system in the San Francisco Bay Area. The system includes 211 kilometers (km) of track, 63 km of tunnels and serves 50 stations across San Francisco, San Mateo, Alameda, Contra Costa, and Santa Clara counties, providing an essential transportation link and offering a convenient alternative to driving that serves many key regional nodes including San Francisco and Oakland airports, downtown Oakland, downtown San Francisco, the Oakland coliseum, and UC Berkeley. The left panel of Figure 1 illustrates the BART system map. Detailed information can be found in BART (2024a). The Berkeley Hills Tunnel, constructed between 1965 and 1967, is an important segment of the BART system, facilitating train travel through the Berkeley Hills and connecting the Rockridge and Orinda stations on the Yellow Line, the longest and most heavily used line. To the west of the tunnel is downtown Oakland, the broader East Bay area, and San Francisco, which comprise the commercial core of the region. To the east is a series of suburban areas containing a large portion of the Bay Area population including Orinda, Lafayette, Walnut Creek, Pleasant Hill, Concord, and Antioch.

Regional Faults

The San Francisco Bay Area is a seismically active region. The right panel of Figure 1 depicts the faults within the BART service area. Active faults, including the San Andreas, Hayward, Rodgers Creek, Calaveras, and Concord, display similar right-lateral horizontal movement and have triggered several significant historical earthquakes (California Geological Survey 2006). The San Andreas and Hayward faults have the largest slip rates and have caused the most significant historical earthquakes. The San Andreas fault, about 12 km southwest of Montgomery Street Station in San Francisco, was responsible for the 1906 San Francisco earthquake with an estimated moment magnitude (**M**) of 7.9 and the 1989 Loma Prieta earthquake (**M** 6.9). The Hayward fault caused an estimated **M** 7.0 earthquake in 1868. These earthquakes resulted in extensive damage across the San Francisco Bay Area.

The United States Geological Survey (USGS) Working Group on California Earthquakes Probabilities (Field et al. 2015) reported that there is a 72 percent probability of one or more **M**≥6.7 earthquakes from 2014 to 2043 in the San Francisco Bay region. The probabilities for the major faults are as follows:

- **Hayward Fault:** 33% probability of an **M** 6.7 or larger earthquake occurring on the combined Hayward and Rodgers Creek fault system.
- **San Andreas Fault:** 22% probability of an **M** 6.7 or larger earthquake on the San Francisco Peninsula segment.
- **Calaveras Fault:** 26% probability of an **M** 6.7 or larger earthquake.
- **Concord-Green Valley Fault:** 16% probability of an **M** 6.7 or larger earthquake.

These results suggest that there is a serious risk the BART system could be subjected to severe ground shaking as well as the ground displacements along the aforementioned major faults from future earthquakes. In particular, the intersection of the Berkeley Hills Tunnel with the Hayward Fault has significant implications for the functionality of the BART system. To better understand the risks of a major event on the Hayward fault and to facilitate planning and preparedness activities, the USGS and its partners developed the **M** 7.0 HayWired scenario (Hudnut et al. 2018). This scenario consists of a rupture extending 84 km along the Hayward Fault, including the segment passing through the Berkeley Hills Tunnel. It is one of 39 simulated earthquakes with magnitudes ranging from 6.6 to 7.2; collectively they underscore the urgent need for thorough planning and preparedness to address such risks (Detweiler and Wein 2017).

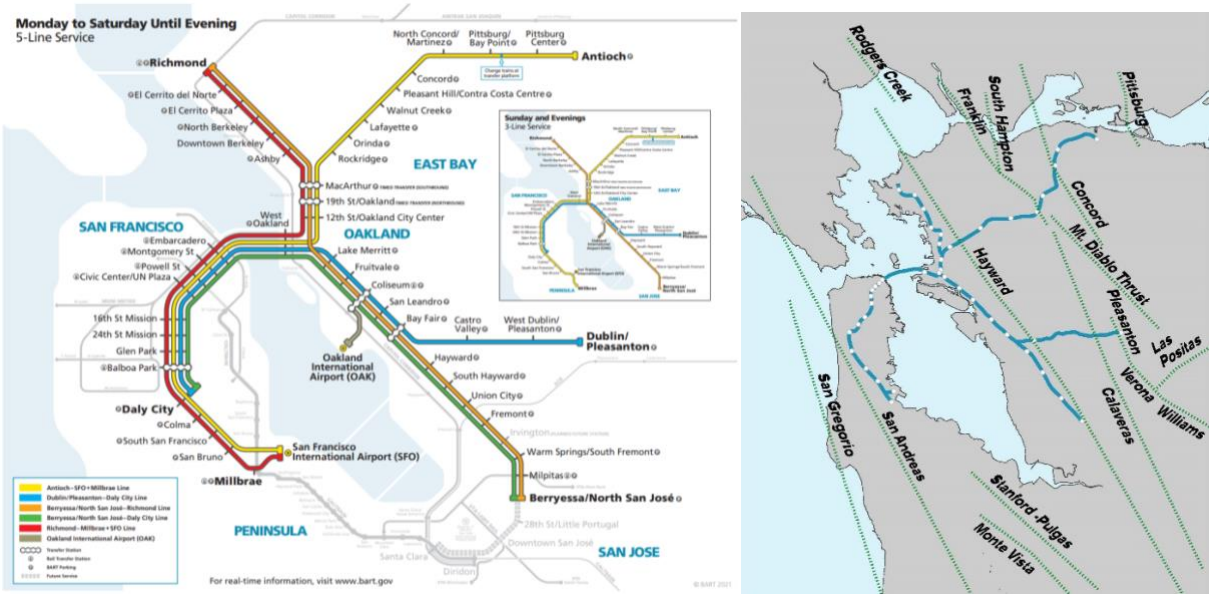

Figure 1. BART system map (left panel), and the Bay Area faults in the BART service area (right panel) (https://www.bart.gov/about/projects/eqs)

BART Retrofit Program

BART initiated its Earthquake Safety Program to prioritize public safety and enhance resilience against significant earthquakes (BART 2024b). A major early effort in this program was a seismic vulnerability assessment to determine how system components would perform during a major earthquake (Bechtel 2000). The scenarios for earthquakes considered in that assessment were as follows: Hayward Fault (**M** 7.0), San Andreas Fault (**M** 8.0), Calaveras Fault (**M** 6.8) and Concord fault (**M** 6.8). The findings showed that, without necessary upgrades, the system might be out of operation for over two years following a severe earthquake. Alternative retrofit options were presented to BART management and were based on the then-current state-of-the art of seismic design. Despite a feasibility study being carried out to explore different retrofit and replacement options, the Berkeley Hills Tunnel was excluded from the retrofit program, as no economically feasible retrofit solution was identified.

BART's Earthquake Safety Program developed site-specific response spectra using horizontal ground motions from Next Generation Attenuation models for a M 7.25 earthquake scenario on the Hayward Fault (Wang et al. 2013). The design basis earthquake ground motion used for retrofit design was determined by selecting the higher of two values: the deterministic median ground motion plus half the standard deviation (which is a predicted shaking level based on seismological parameters plus the uncertainty from a ground motion model), or the probabilistic ground motion with a 500-year return period. For operability retrofits, the lower-level design basis earthquake, based on deterministic median ground motion, was used. Figure 2 depicts the seismic performance objectives of the BART Retrofit Program (City and County of San Francisco 2020). The aim is to upgrade the BART system (including aerial guideways, underground stations, tunnels, and the Transbay Tube) to achieve the following goals:

- Life Safety: Provide life safety by preventing structural collapse during a 500-year seismic event across the entire network.
- Operability: Rapidly restore services and core system (from Daly City Yard to the West Portal of the Berkeley Hills Tunnel and from MacArthur to North Berkeley stations) operability after an earthquake, aiming to minimize service disruption and downtime.
- Modified Operability: Maintain "modified operability" of the rail service from Rockridge to Concord following a deterministic scenario earthquake of **M** 7.25 on the Hayward Fault.
- Long-Term Resilience: Ensure that critical assets remain operational during a 500-year seismic event and provide life safety during a 1000-year seismic event.

Lifelines Restoration Performance Project

The Lifelines Restoration Performance Project, undertaken by the San Francisco Lifelines Council, explored the effects of two extreme scenarios: a **M** 7.9 earthquake on the San Andreas Fault, similar to the 1906 San Francisco earthquake, and a **M** 7.0 earthquake on the Hayward Fault, based on the USGS HayWired scenario (City and County of San Francisco 2020). The goal was to evaluate how these scenario events would impact the regional lifeline systems serving San Francisco, including communications, water, power, and transportation. The project

provided expected restoration timelines for lifeline systems and highlighted the interdependencies among these systems, identifying key actions to meet future recovery targets and improve community-wide recovery planning.

For the "worst-case" scenario involving the Hayward Fault, basic service between downtown San Francisco and Oakland would likely be able to resume within 24 hours. Core system service could be expected to be operational within one to two weeks, with full system restoration occurring within six months. Service on the Richmond line could be restored quickly. However, service on the Antioch line would be seriously disrupted if the Berkeley Hills Tunnel experienced damage due to seismic activity along the Hayward Fault, which could take six months to a year to repair and fully restore service (City and County of San Francisco 2020).

These results highlight that potential earthquake damage to the Berkeley Hills Tunnel could lead to significant service disruptions that could strain alternative transportation options and impact the broader transit network in the Bay Area. Quantifying the extent of damage is crucial for effective planning and service restoration. Understanding the severity of the damage allows for accurate estimates of the time required to restore services, which in turn supports better decision-making and resource allocation for efficient recovery and reducing impacts on the transit system.

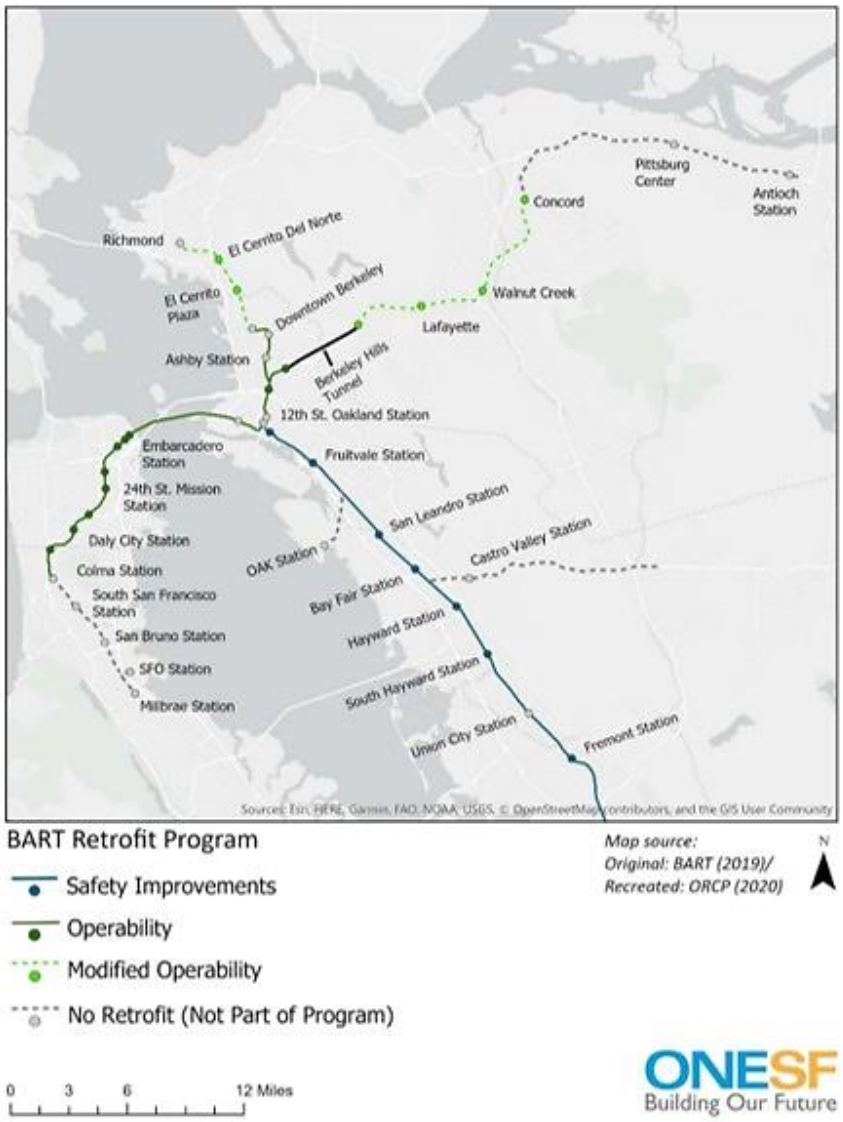

Figure 2. Seismic Performance Objectives for BART Retrofit Program (City and County of San Francisco 2020).

BART Berkeley Hills Tunnel

The Berkeley Hills Tunnel, comprising twin bores each approximately 5 km in length, pass through the Oakland-Berkeley Hills between the Rockridge and Orinda stations. Each tunnel has an inner diameter (D_{inner}) of 5.33 meters (m) and a liner thickness of 0.455 m. The two bores, which are 30 m apart, intersect the Hayward Fault approximately 300 m from the west portal of the tunnels. To sustain significant rock loads, the two tunnels were designed with a circular reinforced concrete (RC) liner, even though they were excavated in a horseshoe shape. The RC liner of the tunnels includes two layers of longitudinal steel reinforcement at the top and bottom levels,

along with stirrups for shear. Figure 3 shows the cross-section of one tunnel and the reinforcement layout. The concrete used in the tunnels has a design compressive strength of 20 Megapascals (MPa). The reinforcement steel is U.S. Grade 40, with a design yield strength of 275 MPa and an ultimate strength of 380 MPa. In this study, the longitudinal reinforcement ratio (indicating the proportion of steel within the concrete cross-section) was 1.5 percent, consisting of #9 bar stirrups (diameter of approximately 29 mm) spaced at 305 mm.

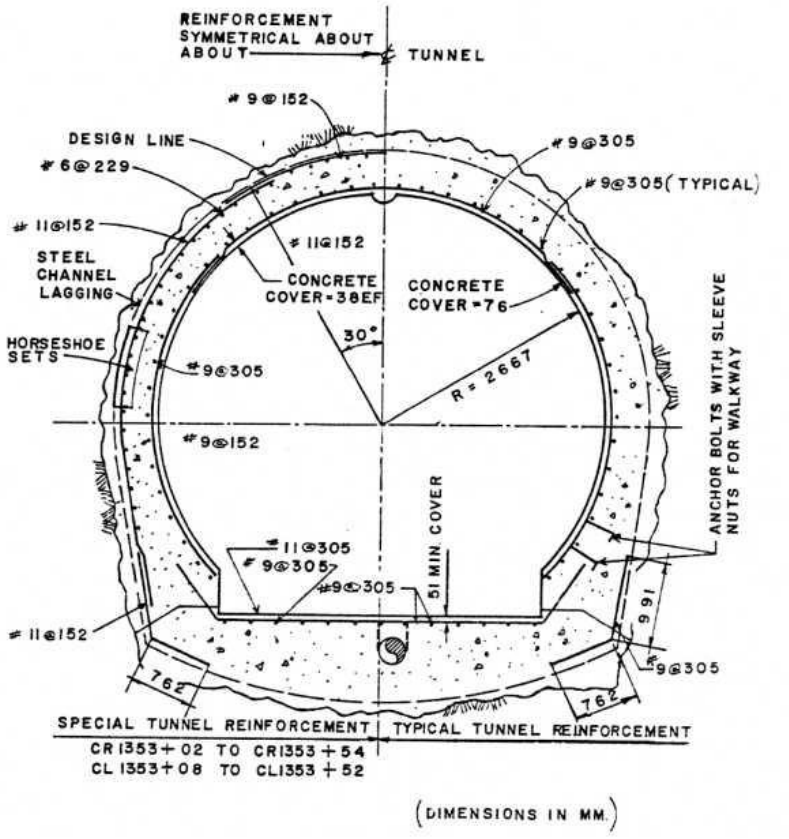

Figure 3. Cross section of the Berkeley Hills Tunnel (from Brown et al. 1981).

Geological Formation Along the BART Tunnel

The Berkeley Hills Tunnel traverses a complex geology significantly impacted by the Hayward Fault. As shown in Figure 4, the tunnel crosses various rock types, beginning on the west end with the Franciscan formation, which is characterized by sandstone, shale, and sheared volcanic rocks, alongside Quaternary sediments. The fault zone includes distinctive serpentine gouge, which is a soft, clay-like material formed from ultramafic rock, and fault gouge, a mix of crushed rock and fine sediment. East of the fault, the geology features serpentinite with metabasalt inclusions, which becomes less deformed further from the fault (Ayres 1969, Blake et al. 1974, Geomatrix Consultants 2001). This study specifically examines the 240 m section of the west portal of the tunnel that intersects the Hayward Fault zone, with further details discussed in subsequent sections.

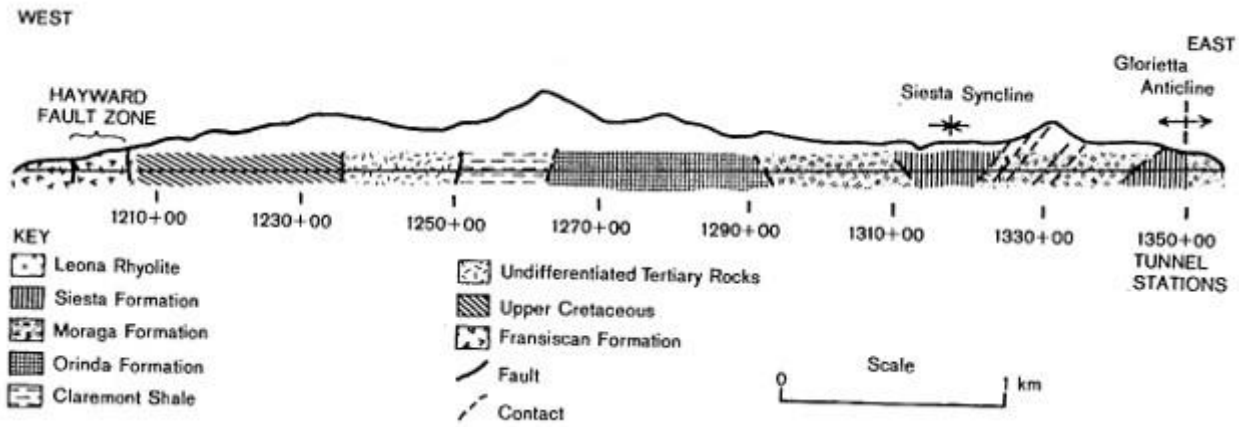

Figure 4. Geological formation along the BART tunnel through Berkeley Hills (after Bechtel 1968).

Creep Displacement of the Hayward Fault and Crack Patterns in the Tunnel

The Hayward Fault shows creep behavior with a slip rate ranging from approximately 3 to 7 millimeters per year (mm/yr), though higher rates are seen at Fremont, California (Lienkaemper et al. 1997, Bürgmann et al. 1998). Lienkaemper and Galehouse (1997) reported a creep rate of 3.4 mm/yr at the BART tunnel level. Creep displacement on the Hayward Fault helps relieve stress buildup that could otherwise lead to more frequent earthquakes, thereby affecting the seismic hazard curve. During the original construction of the tunnel, BART issued a change order to the track construction contract that replaced the concrete ties with wooden ties to allow for the track realignment across the Hayward fault zone during creep (or fault) displacement (Brown et al. 1981).

To monitor deformations and load changes in the tunnel lining in the Hayward Fault zone, pressure cells and rock movement indicators (RMIs) were installed in 1967. Figure 5 shows their locations, as well as the section of the tunnel affected by the fault and the surrounding geology. Previous investigators concluded that fault creep movements were occurring in a narrow 183 m zone between Stations 1198+00 and 1204+00 (Bechtel 1970). In July 1979, BART conducted a comprehensive assessment of tunnel cracking to determine the impacts of 10 years of creep displacement from 1969 to 1979. The investigation spanned 585 m from Station 1191+00 to Station 1210+20, which included both areas affected by fault movements and adjoining areas that are not affected, so that different patterns of concrete cracking could be identified and differentiated. The investigations showed that most cracks were vertical and aligned perpendicular to the tunnel axis. These cracks predominantly ended above the tunnel invert (the lowest part of the tunnel), suggesting that concrete shrinkage was likely the main cause (from Station 1191+00 to Station 1210+20, see Appendix D of Brown et al. 1981). However, some cracks might have been linked to axial strains from lateral displacements along the Hayward Fault. Circumferential cracking, typically occurring at 3 to 4 m intervals, was observed, with many cracks being significantly wide, indicating fault-induced movements. Additionally, longitudinal cracks between the sidewalls and tunnel crown were noted between Stations 1202+60 and 1203+25, and were attributed to significant lateral ground pressures that led to high bending stresses. A specific pattern of low-angle cracks, stretching from the tunnel crown to the

invert between Stations 1200+60 and 1201+10, was attributed to right-lateral fault displacement within a fault shear zone, as shown in Figure 5.

a)

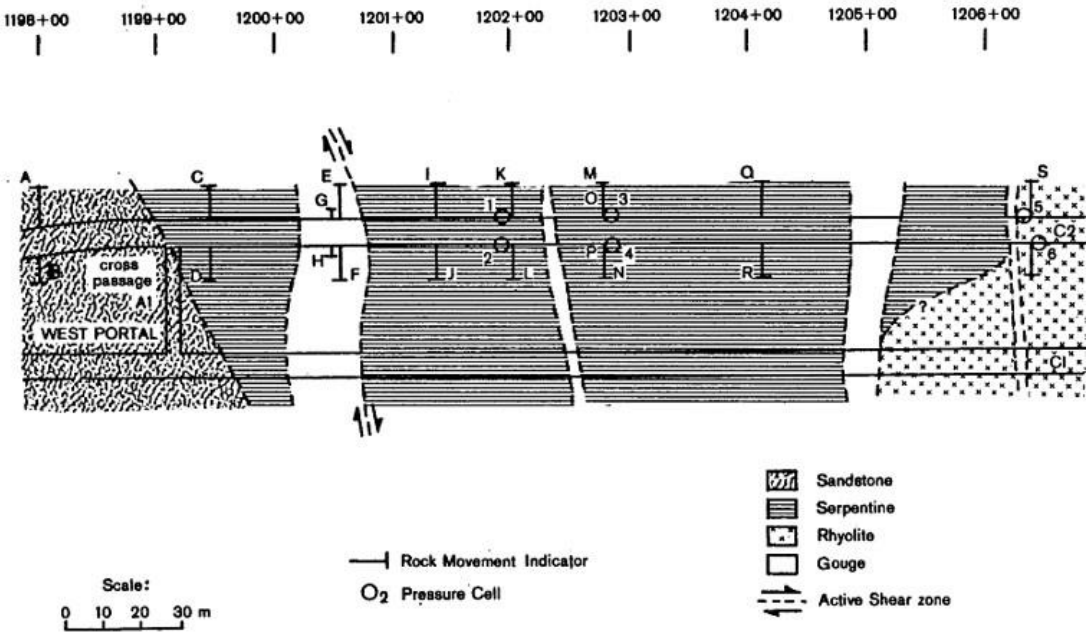

b)

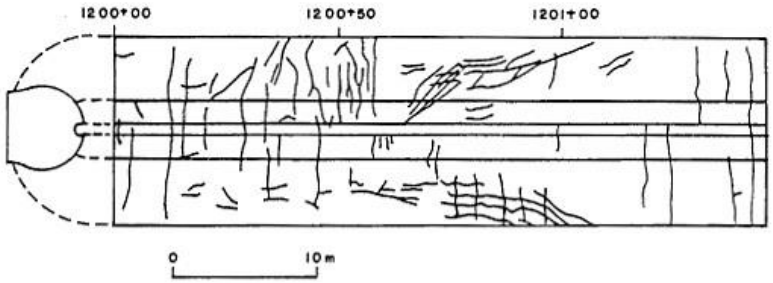

Figure 5. a) Section of tunnel in Hayward Fault zone, surrounding rocks and location of instrumentation, b) Liner crack pattern for 10 years (1969-1979) of creep displacement (Brown et al. 1981).

Tunnel Computer Modeling Approach

A three-dimensional (3D) FEM model was developed using ABAQUS software to analyze one tunnel bore and its surrounding rock (Dassault Systèmes Simulia Corp. 2020). Figure 6a illustrates the 3D FEM model of the tunnel extending along the Z-direction (longitudinal) with a length of 240 m, embedded in sandstone, serpentine, and gouge. Model dimensions are 200 m in height, 50 m in width, and 240 m in length, with the tunnel centered at a height of 100 m to reflect its actual in-situ condition. The length of the model was selected to span across the zone of fault rupture with zones without concentrated shear deformations at each end of the model.

Figure 6b depicts the tunnel cross-section, highlighting the crown at the top, the invert at the bottom, and the left and right walls. Given that the twin tunnels are separated by 30 m, it is assumed that they do not significantly interact with each other. The fault zone, characterized by gouge material, is 25 m in length (as measured in the Z-direction). The model includes a zero-length (as measured in the Z-direction) fault plane at the location shown in Figure 6a, corresponding to the contact surface between the gouge and serpentine. The location of the fault plane was determined based on the alignment between observed creep cracks in the tunnel liner and the tension damage distributions obtained from the analysis, as discussed in the following section. A fault dip angle of 90° was assumed to simulate strike-slip conditions.

Both the rock mass and tunnel lining were modeled using C3D8R eight-node linear hexahedral solid elements (Dassault Systèmes Simulia Corp. 2020). The steel reinforcement was represented using 2-node linear 3D truss elements (T3D2) with a bilinear elastoplastic material model and was embedded within the concrete lining. To improve computational accuracy, finer meshes were applied within 5 m of each side of the fault plane, with a mesh size of approximately 0.5 m in the longitudinal direction. Beyond this range, the mesh size increased to 3-4 m. In ABAQUS, the interaction between rock surfaces and rock-tunnel interfaces was modeled as "hard contact" in the normal direction, meaning that if the normal contact pressure exceeded the frictional resistance, the surfaces could not interpenetrate. The tangential direction is parallel to the contact surface, either horizontally between rock layers or circumferentially around a tunnel lining. In this case, a penalty function method was used to simulate shear behavior (Laursen 2002). This approach prevented excessive sliding to more accurately reflect shear behavior. The friction coefficient, μ, was essential for this model, as it determined the maximum shear stress before sliding occurred. According to Coulomb's law, shear stress (τ) was calculated as the μ multiplied by the normal stress (σ). In this study, the tangential contact was defined using a friction coefficient of $\mu = 2/3\tan(\phi) = 0.4$, where ϕ represents the internal friction angle of the rock material.

The surrounding rock masses were represented using an elastic-perfectly plastic Mohr-Coulomb constitutive model, which is characterized by an elastic modulus (E) and Poisson's ratio for elastic behavior and an internal friction angle and cohesion (c) intercept to define the yield surface and failure criterion. It was assumed that the dilatation angle is zero, indicating that the material undergoes shear deformation without volume change. Table 1 lists the mechanical properties of the surrounding rock, with elastic modulus values obtained from Brown et al. (1981).

As previously noted, our numerical model assumes that fault rupture occurs at the intersection of the fault zone (i.e., gouge) with the serpentine. The section adjacent to the fault plane is designated as the moving block, where displacement is applied. The fault displacement is applied in the positive x-direction both to the bottom of the moving block and its vertical plane (see Figure 6a). The lateral boundaries of both the fixed and moving blocks were restrained in the normal direction. The bottom surfaces of the blocks were fixed in the vertical (i.e., y-axis) direction.

a)

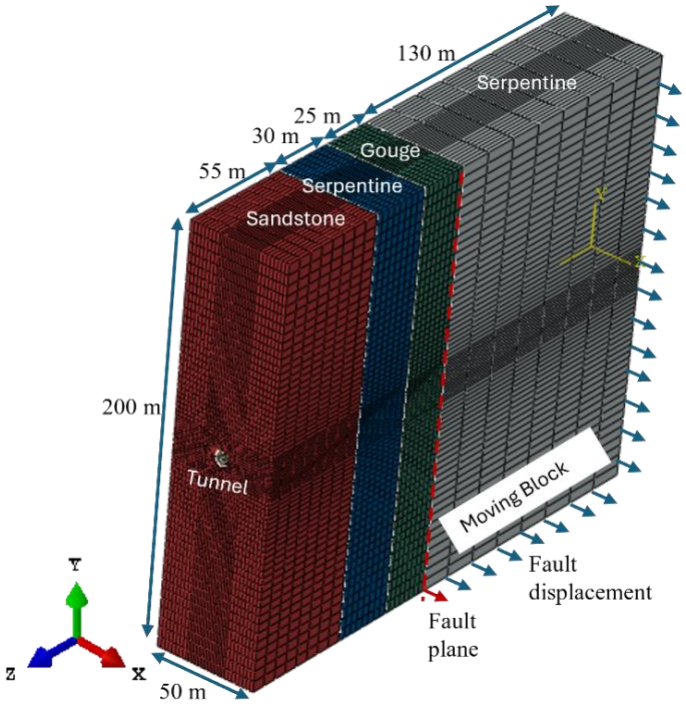

b)

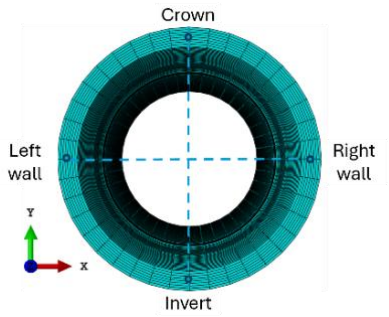

Figure 6. a) 3D ABAQUS finite element model of the tunnel b) tunnel cross-section, highlighting the crown at the top, the invert at the bottom, and the left and right walls.

Table 1. Mechanical properties of the surrounding rock.

Rocks	Mass Density (kg/m³)	Elastic Modulus, E (MPa)	Poisson's ratio	Inner Friction Angle, φ (°)	Cohesion, c (MPa)
Sandstone	2600	9000	0.25	30	10
Serpentine	2600	3400	0.30	36	3.7
Gouge	2600	1000	0.40	26	0.5

Theoretical Background for Concrete Damage Plasticity Model

The Concrete Damage Plasticity (CDP) model (Lubliner et al. 1989) is a framework used to simulate the behavior of concrete under various loading conditions. This model is based on three main concepts:

1. Yield Surface: This concept extends the idea of "yield load" by defining a surface in stress space that represents the transition from elastic to inelastic behavior. It helps in assessing whether the material remains in its elastic state or starts to deform plastically under applied stresses.

2. Flow Rule: This defines how the material undergoes inelastic deformation once it exceeds the yield surface. It describes the relationship between the stresses and the plastic strains that develop when the material transitions from elastic to inelastic behavior.

3. Hardening Rules: These rules describe how the yield surface and flow rule evolve as the material undergoes inelastic deformations. They help in understanding how the material's response changes with continued loading, including changes in stiffness and strength due to damage accumulation.

These concepts together provide a comprehensive approach for modeling the behavior of concrete, particularly in capturing both damage and plastic deformation, which is important for accurate simulations of tunnel response. The CDP model also uses several plastic parameters to characterize material behavior. Table 2 summarizes the CDP plastic parameters adopted in this study.

Table 2. CDP plasticity parameters.

Parameter	Description	Value
Dilatation angle (°)	Defines the degree of volumetric expansion during shear.	35
Eccentricity	Determines the shape of the yield surface, influencing how plastic deformation progresses.	0.10
f_{bo}/f_c	Represents the ratio of initial equibiaxial compressive yield stress to initial uniaxial compressive yield stress.	1.16
K	Indicates the increase in yield surface size with plastic deformation.	0.66
Viscosity	Describes the material's response to dynamic loading conditions.	0.005

The CDP model characterizes inelastic behavior of the concrete by defining damage factors for compression and tension, focusing on failure modes like cracking and crushing. It tracks the evolution of the yield surface through compressive and tensile equivalent plastic strains ($\tilde{\varepsilon}_c^{pl}$ and $\tilde{\varepsilon}_t^{pl}$). The model ensures that the input inelastic strain ($\tilde{\varepsilon}_c^{in}$) is positive and increases with the damage factor. Figure 7 illustrates the uniaxial compression and tension stress-strain curves of the CDP. For the compression behavior, we employed the Kent and Park parabolic constitutive material model to define the behavior of the unconfined concrete (Kent and Park 1971). The relevant strain parameters were computed using the following equations:

$$\tilde{\varepsilon}_c^{in} = \varepsilon_c - \varepsilon_{0c}^{cl} \quad (1)$$

$$\varepsilon_{0c}^{cl} = \frac{\sigma_c}{E_0} \quad (2)$$

$$\tilde{\varepsilon}_c^{pl} = \tilde{\varepsilon}_c^{in} - \frac{d_c}{(1-d_c)}\frac{\sigma_c}{E_0} \quad (3)$$

where $\tilde{\varepsilon}_c^{in}$ represents the compressive inelastic strain, ε_{0c}^{cl} is the elastic strain at the initial elastic modulus (E_0), d_c is the compression damage factor. The parameter d_c quantifies the reduction in the compressive strength of concrete relative to its ultimate compressive strength, given by $1-\sigma_c/\sigma_{c,r}$, where $\sigma_{c,r}$ is the ultimate compressive strength.

Tensile behavior starts with a linear-elastic phase, then softens until failure. This study adopted the softening curve suggested by Allam (2013). The tensile strength capacity (σ_{t0}) was calculated using the formula $0.7\sqrt{\sigma_{c,r}}$ (in MPa) (ACI 318-19). The strain parameters can be determined using the following expressions:

$$\tilde{\varepsilon}_t^{ck} = \varepsilon_t - \varepsilon_{0t}^{cl} \quad (4)$$

$$\varepsilon_{0t}^{cl} = \frac{\sigma_t}{E_0} \quad (5)$$

$$\tilde{\varepsilon}_t^{pl} = \tilde{\varepsilon}_t^{ck} - \frac{d_t}{(1-d_t)}\frac{\sigma_t}{E_0} \quad (6)$$

Here, $\tilde{\varepsilon}_t^{ck}$ denotes the tensile cracking strain, ε_{0t}^{cl} is the tensile strain at the initial elastic modulus E_0, $\tilde{\varepsilon}_t^{pl}$ represents the tensile plastic strain. d_t is the tensile damage parameter that quantifies stiffness loss and crack growth in tension. It can be obtained using the formula $1-\sigma_t/\sigma_{t0}$, where σ_{t0} is the tensile strength of the concrete.

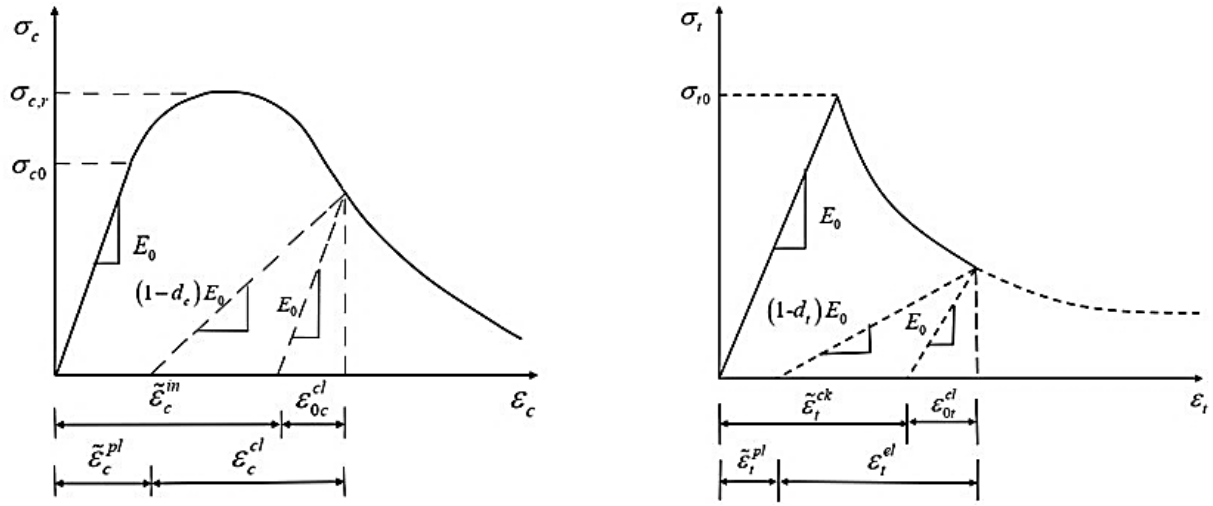

Figure 7. Uniaxial compression (left panel) and tension (right panel) stress-strain curves of CDP (Dassault Systèmes Simulia Corp., 2016)

Figure 8 illustrates the stress-inelastic strain relationships and damage factors for both compression and tension of C20 concrete, as implemented in the CDP model in ABAQUS software. Henceforth, the compression and tension damage parameters will be referred to as DAMAGEC and DAMAGET, respectively. As seen, the DAMAGEC and DAMAGET increase until they reach values of 0.6 and 0.8, respectively. This indicates that the parameters achieve their maximum inelastic strains when the concrete retains 40 percent of its original compressive strength and 20 percent of its tensile strength.

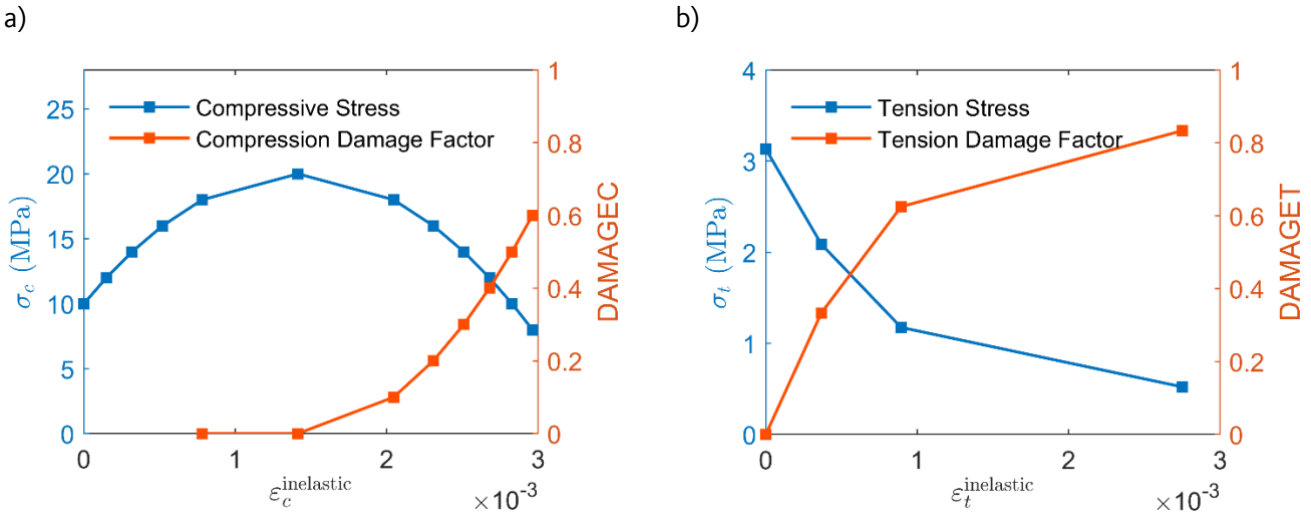

Figure 8.a) Compression and b) tension stress-strain relationships and damage factors for C20 concrete adopted in the model.

Analysis Procedure

The analysis started with a geostatic analysis to establish the initial stress conditions due to gravity. In this step, the model was configured with the soil domain, and gravity was applied as a body force to simulate the self-weight of the soil. Contact interactions between the soil and the tunnel were deactivated to isolate the soil's response to gravity alone. The in-situ stresses within the soil were computed and used as the initial stress state (i.e., Predefined field: stress, in the ABAQUS software) during the gravity analysis of the tunnel. In the gravity analysis step, the tunnel geometry was introduced into the model and contact interactions between the soil and the tunnel were reactivated and the tunnel weight was applied to the model. In the final step, fault displacement was applied incrementally in a quasi-static manner, meaning it was introduced in small increments to approximate static conditions. This way, we ensured that the analysis captured the tunnel response to fault displacement without the influence of dynamic effects.

Validation of the Numerical Model

To validate the numerical model, we compared the crack patterns observed in the tunnel liner with the simulated tensile cracking patterns of the lining under a 10-year creep displacement of 0.04 m, corresponding to a creep rate of 4 mm/yr, as shown in Figure 9. As noted previously, Brown et al. (1981) identified 45-degree surface cracks in the liner that were attributed to creep-induced displacement, which were located primarily in the moving block section and extended into the fault zone over a distance of 8 m. For the numerical results, we utilized DAMAGET to assess the damage in the tunnel lining.

The analysis revealed that the DAMAGET parameter peaked at approximately 0.25 in the sidewalls and 0.15 at the crown, suggesting the onset of minor to moderate cracking in these regions. Cracks on the right wall extended from the fault plane towards the moving block, while cracks on the left wall were more pronounced near the fault plane. At this creep displacement level, no compression damage (DAMAGEC) was observed. The crack pattern in the tunnel model closely matched the observed cracks in terms of both location and length along the tunnel axis. The consistency of these results demonstrates that the numerical model is reliable for simulating tunnel behavior under small fault displacements, which is a useful starting point for simulating large displacements for which validation is not possible.

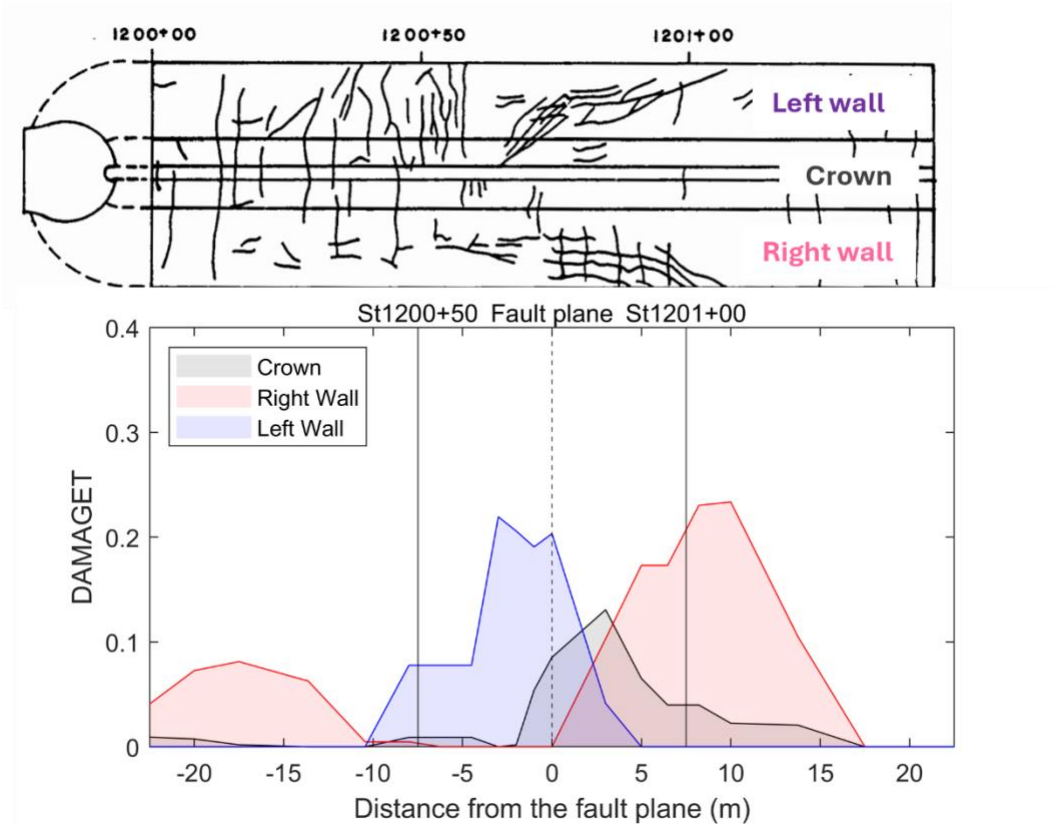

Figure 9. Comparisons of the crack patterns observed in BART tunnel with the simulated tensile cracking patterns of the concrete tunnel liner under a 10-year creep displacement of 0.04 m.

Assessing Tunnel Structural Damage Under Fault Displacement and BART System Resilience

This section describes a detailed analysis of tunnel deformation under varying fault displacements. We begin by employing Fault Displacement Hazard Initiative (FDHI) models to develop fault displacement hazard curves. We identify how these fault displacements influence horizontal displacement of both the tunnel and the surrounding rock. We present longitudinal strains at critical locations, including the crown, invert, and side walls. We investigate bending damage through curvature analysis and examine shear strain distributions. Utilizing the Concrete Damage Plasticity (CDP) material model, we quantify damage by integrating compression and tension damage parameters. Based on the damage estimates, post-event functionality and restoration timelines of the BART tunnel are estimated.

Probabilistic Fault Displacement Hazard Analysis

To estimate the probability of fault displacements in general, and for the Hayward Fault in particular, two elements are needed (e.g., Youngs et al. 2003): (a) fault displacement predictive models providing the median estimate of the fault displacement, and the associated variability, based on parameters like earthquake magnitude and focal mechanism, and, (b) an earthquake recurrence relationship for the fault that expresses the time rate of earthquakes as a function of magnitude. The combination of elements (a) and (b) allows for a comprehensive assessment of fault displacement hazards, making it the preferred method for evaluating risks associated with critical infrastructure.

For item (b) above, we used the earthquake rupture forecast model provided by the USGS, which is known as the UCERF3 model (Field et al. 2015). This model provides the geometry and rate of seismic activities of major known faults in California, including the Hayward Fault. Regarding item (a), scaling relationships can be used to estimate the mean and standard deviations of displacement on fault traces. Early models for such relations for principal fault traces are presented by Wells and Coppersmith (1994) (all fault types), Moss and Ross (2011) (reverse faults), and Petersen et al. (2011) (strike-slip faults). More recent models have been prepared using a larger database developed in the FDHI research program (Fault Displacement Hazard Initiative — The B. John Garrick Institute for the Risk Sciences (ucla.edu)) that includes 75 historical surface-rupturing crustal earthquakes, with magnitudes ranging from **M** 4.9 to 8.0 (Sarmiento et al. 2024a). The FDHI Program was a major initiative involving numerous researchers and practicing professionals addressing challenging technical issues on fault displacements. Under the FDHI Program, four new fault displacement predictive models were developed. Comparisons of these four new FDHI predictive models are provided in Sarmiento et al. 2024b.

Combining two FDHI predictive models (Lavrentiadis and Abrahamson 2023, LA23; and Kuehn et al. 2024, KEA24) for strike-slip faults, such as the Hayward Fault, and an existing model (Petersen et al 2011; PEA11) along

with the UCERF3 earthquake rupture forecast model, probabilistic fault displacement hazard at the cross section of the BART tunnel and Hayward Fault can be computed. Figure 10 illustrates fault displacement hazard curves for the BART tunnel site crossing the Hayward fault, derived from these predictive models. Note that these scaling relations, and the hazard analyses, consider only principal fault displacements and not secondary features located off the main fault. The results demonstrated that all three models produced similar hazard curves. Given a fault displacement level, one can determine the return period by calculating the inverse of the mean annual rate of exceedance of that displacement. Specifically, the return period (T in units of years) is given by T =1/λ, where λ represents the mean annual rate of exceedance of the fault displacement. Additionally, the mean probability of fault displacements (P) exceeding a given threshold over the tunnel's lifespan (t) can be estimated assuming a Poisson Process as:

$$P = 1 - e^{-\lambda t} \tag{7}$$

These hazard metrics can be crucial for designing and assessing risks associated with tunnel displacements over a 50-year or 100-year life span. The risk metrics for the fault displacement levels analyzed in this study are addressed in the subsequent section.

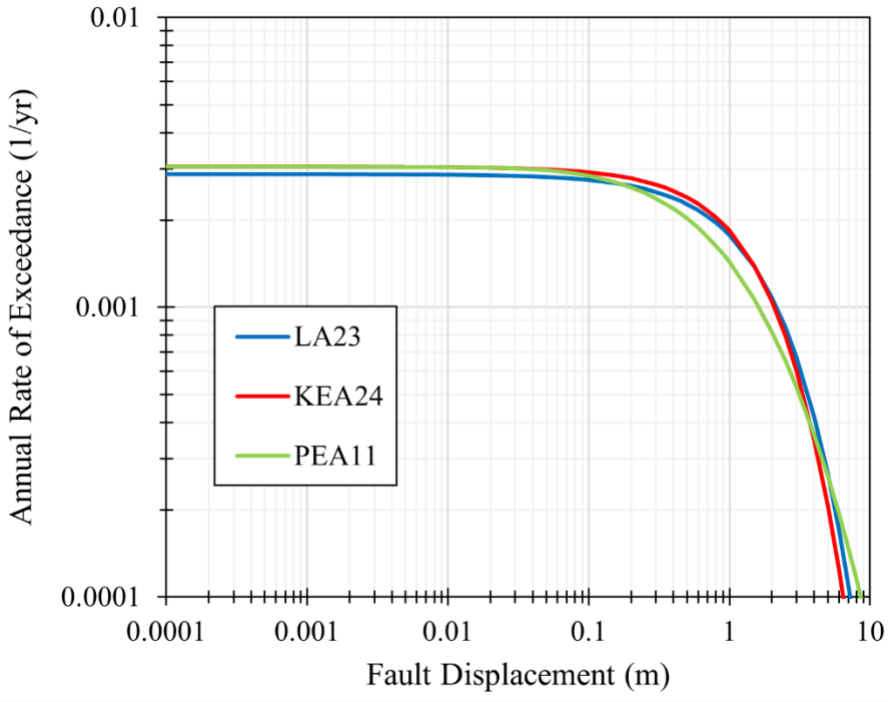

Figure 10. Fault displacement hazard curves from LA23 and KEA24 models (Courtesy: Thompson, Zandieh, Sarmiento, 2024)

Deformation Characteristics

Displacement Responses

Figure 11a compares the profiles (i.e., variation of displacement with location in the Z-direction) of the horizontal displacements for the right walls of the tunnel and the surrounding rock (i.e., free-field) under a fault displacement (δ) of 1.5 m. It was observed that the surrounding rock reached its maximum δ level at the fault plane, while the horizontal displacement of the tunnel gradually increased between the fault zone and the moving block. A slight horizontal movement was noted within the fault zone in the fixed block, as lateral movement was allowed. To better illustrate the change in the horizontal displacement of the tunnel along its longitudinal direction, we plotted in Figure 11b the displacement gradients (dx/dz) for δ values of 0.2, 0.5, 1.0, and 1.5 m. For all δ levels, the displacement gradient increased within 5 m of the fault zone, steepened sharply after crossing the fault plane, peaked within 4 m on the moving block side, and then gradually decreased over the next 8 m. A total length of approximately 10 m, where variations in slope were observed in the displacement gradient, can be considered an area of stress and strain localization as well as a shear zone.

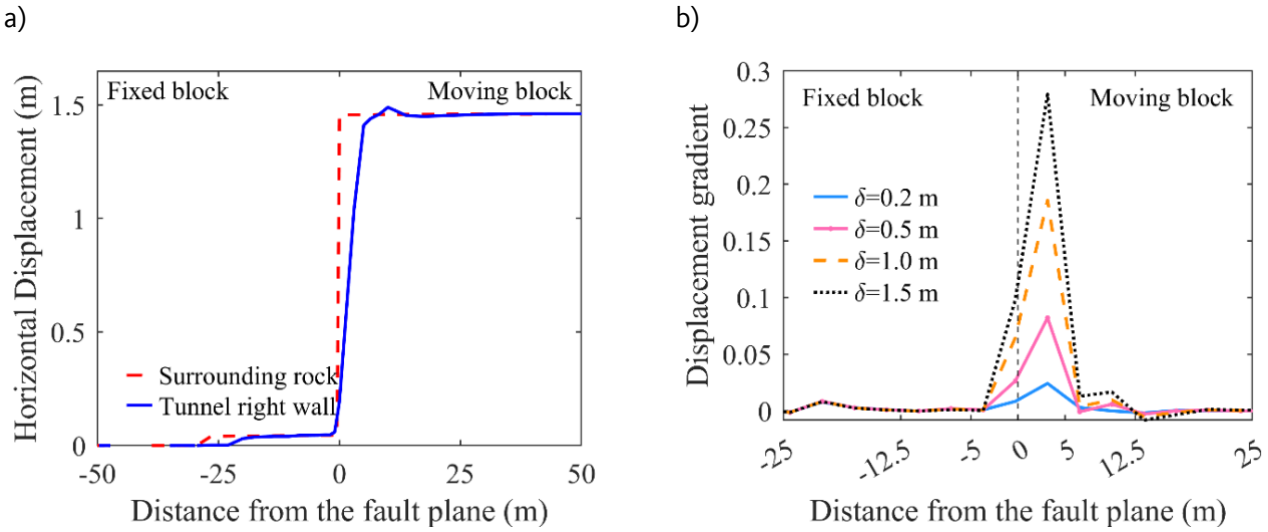

Figure 11. a) Horizontal displacement profiles of the right wall of the tunnel and the free-field rock for a fault displacement of 1.5 m, b) Displacement gradients under various fault displacement levels.

Strain Distributions Under Various Fault Displacements

Figure 12 presents the longitudinal (Z-direction) strains observed in the crown, invert, left and right walls of the tunnel lining, at various δ levels. The strain values provided in this figure represent the average of the strains in the inner and outer sections of the lining. In that regard, the inner section refers to locations visible inside the tunnel, while the outer sections are those in contact with the surrounding rock. Note that negative values denote compression, while positive values represent tension. Results are shown for a 100-m length of the tunnel, centered around the fault plane. As shown in Figure 12, fault displacement significantly affected the structural

response of the lining over an approximate length of 20-30 m, while the influence decreased beyond 25 m from the fault plane in both directions. Strains from fault displacement were mostly concentrated near the fault plane and generally increased as the fault displacement increased. The crown and invert of the tunnel experienced compression strains for $\delta > 0.2$ m. However, minor tension strains were observed at $\delta = 0.2$ m. The peak compressive strains were observed within 4 m of the fault plane, on the moving block side, which is consistent with the observed increase in the displacement gradient. The left and right walls of the tunnel showed varying strain patterns depending on the bending behavior of the tunnel. Specifically, the left wall had tensile strains in the fixed block and compressive strains in the moving block, with the strain profiles being almost symmetric. In contrast, the right wall showed the reverse pattern, with compressive strains in the fixed block and tensile strains in the moving block. In all regions of the tunnel, the most significant increases in strain occurred when $\delta > 0.5$ m. The results indicated that the ultimate limit of tensile strain was exceeded when $\delta \geq 0.2$ m, while the ultimate limit of compressive strain was exceeded when $\delta \geq 1.0$ m.

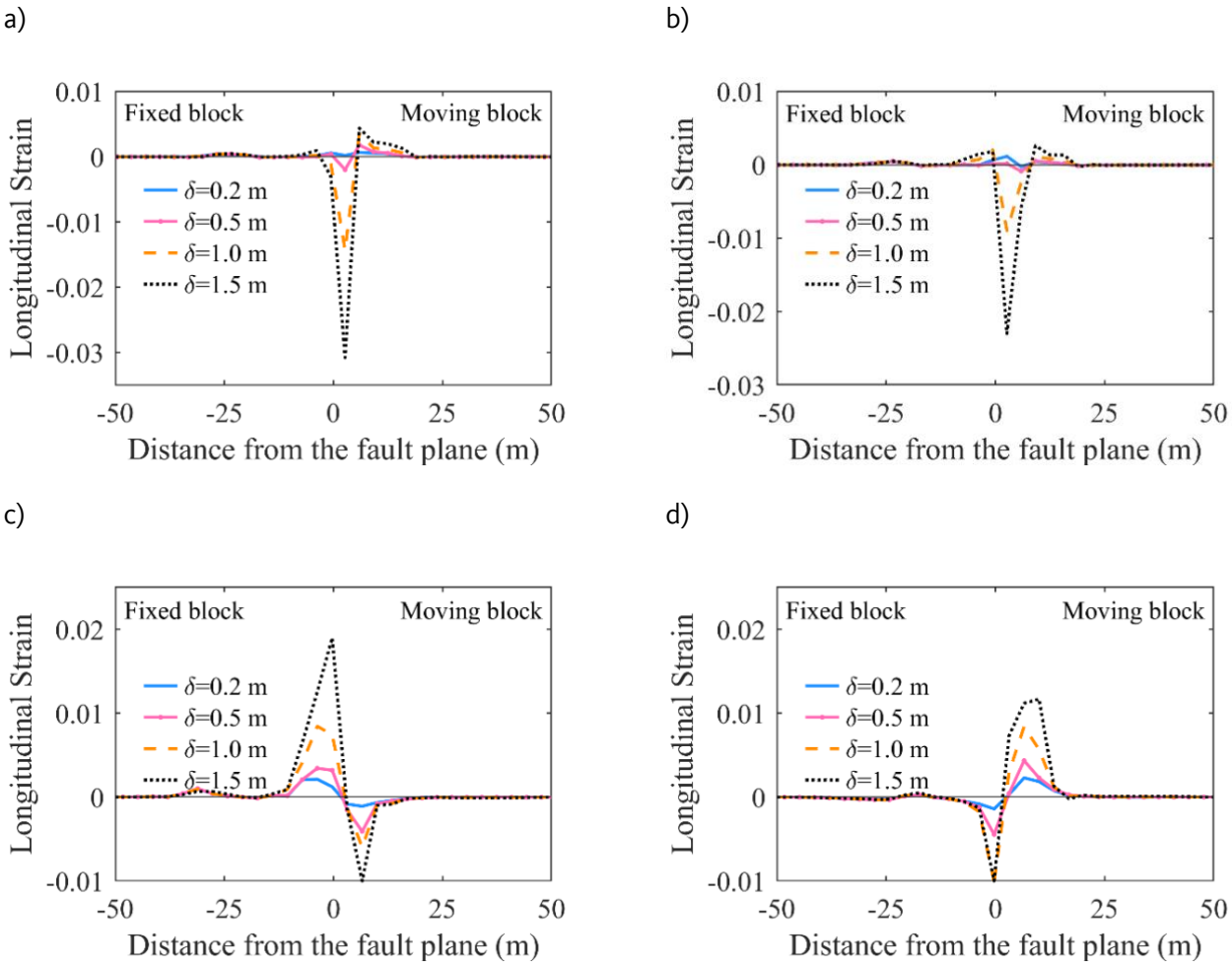

Figure 12. Longitudinal strain distributions along the tunnel axis at various fault displacement levels: a) crown, b) invert, c) left wall, d) right wall of the tunnel. Positive in tension, negative in compression.

Tunnel Section Curvature

To quantify the bending demands applied to the tunnel from fault displacement, we utilized the curvature parameter. Peak curvature is often used as a design parameter due to its relationship with bending moment. It can also serve as an effective indicator of structural damage related to inelastic bending deformations. In the 3D numerical analysis, curvature was estimated as $(\varepsilon_r - \varepsilon_l)/D_{avg}$, where ε_r and ε_l represent the average longitudinal strains at the right and left walls of the tunnel, respectively, and D_{avg} is the average diameter of the tunnel, calculated as $(D_{outer} + D_{inner})/2$. Figure 13 illustrates the curvature profile along the tunnel axis (i.e., variation of curvature in the Z-direction). A negative curvature corresponds to tensile strains along the left wall of the tunnel, while positive curvature indicates tensile strains along the right wall of the tunnel. The peak curvature (i.e., -5×10^{-3} for δ =1.5 m) was observed at the fault plane. Due to its S-curve shape, positive peaks were observed 10 m from the fault plane in the moving block.

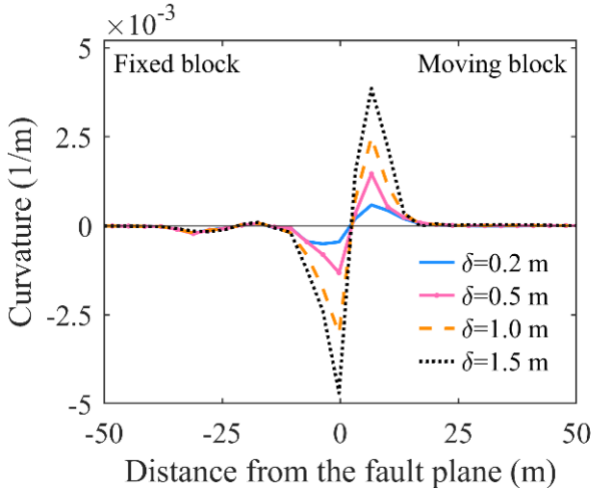

Figure 13. Curvature profile along the tunnel axis.

Shear

During major earthquakes, shear failure is a common mode of structural failure in underground structures that cross active faults (Zhang et al. 2020). To evaluate the demands on the tunnel section from shear, we computed shear strain distributions along the tunnel axis at various fault displacement levels for the crown and invert regions, as shown in Figure 14. To evaluate the damage potential of these strain demands, it is necessary to estimate the shear strain capacity (ε_s), beyond which shear failure is expected. To estimate the shear strain capacity, the shear strength of the concrete (τ) was first assumed to be 10 percent of the compressive strength (Shi 1999). The shear modulus of concrete (G) was computed using ACI 318-08 guidelines. ε_s was then calculated as $\varepsilon_s = \tau/G$ or approximately 0.024 percent. Based on this estimate of capacity, ε_s was exceeded for δ > 0.2 m, suggesting that that the lining may suffer shear cracks and damage due to fault displacement. The peak shear strains were observed at a distance of approximately $1D_{outer}$ from the fault plane on both the fixed block for the crown and the moving block for the invert. The overall structural damage characteristics of the tunnel were

evaluated by considering the combined effects of compression, tension, and shear damage in the concrete as well as the stresses in the steel reinforcement, as discussed in subsequent sections.

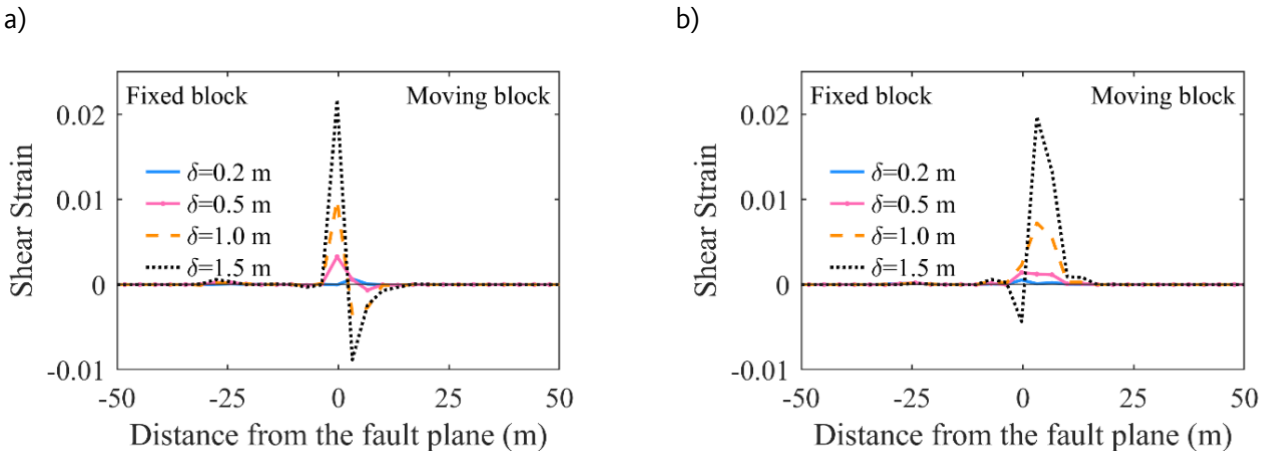

Figure 14. Figure 14. Shear strain distributions along the tunnel axis at various fault displacement levels: a) crown, b) invert. (units in decimal format)

Tunnel Lining Stresses

3D Distributions of Stresses

Figure 15 depicts the patterns of maximum and minimum principal stresses, shear stresses in the tunnel lining, and the Von Misses stresses of the steel bars along the tunnel axis under a fault displacement of 1.5 m, covering a 50 m section centered symmetrically around the fault plane (± 25 m). The maximum principal stress, representing the maximum tensile stress in the lining, was observed in the crown, reaching about 5.8 MPa near the fault plane in the moving block. The next largest maximum principal stresses were in the left and right walls, where the stresses were approximately 4.5 MPa in the areas where the maximum tensile strains occurred. Even though the crown and invert were under compressive longitudinal strain, the combined stress state at the crown, considering both the normal and shear components, resulted in the maximum principal stress being tensile. The minimum principal stress (in compression) of -73 MPa occurred at the sidewalls (outer wall) in the moving block, followed by the crown and invert. These stress levels significantly exceeded the ultimate compressive strength of concrete (20 MPa). Maximum shear stress occurred near the fault plane at the crown, aligned with fault movement, while the invert experienced significant shear stress in the opposite direction. For the reinforcement steel, Von Misses stresses exceeded the yield stress level but did not reach the rupture stress of 385 MPa. The zone within the tunnel section where steel reinforcement yielding was expected to extend approximately 25 m on either side of the fault plane, based on the locations of high-tension stress areas.

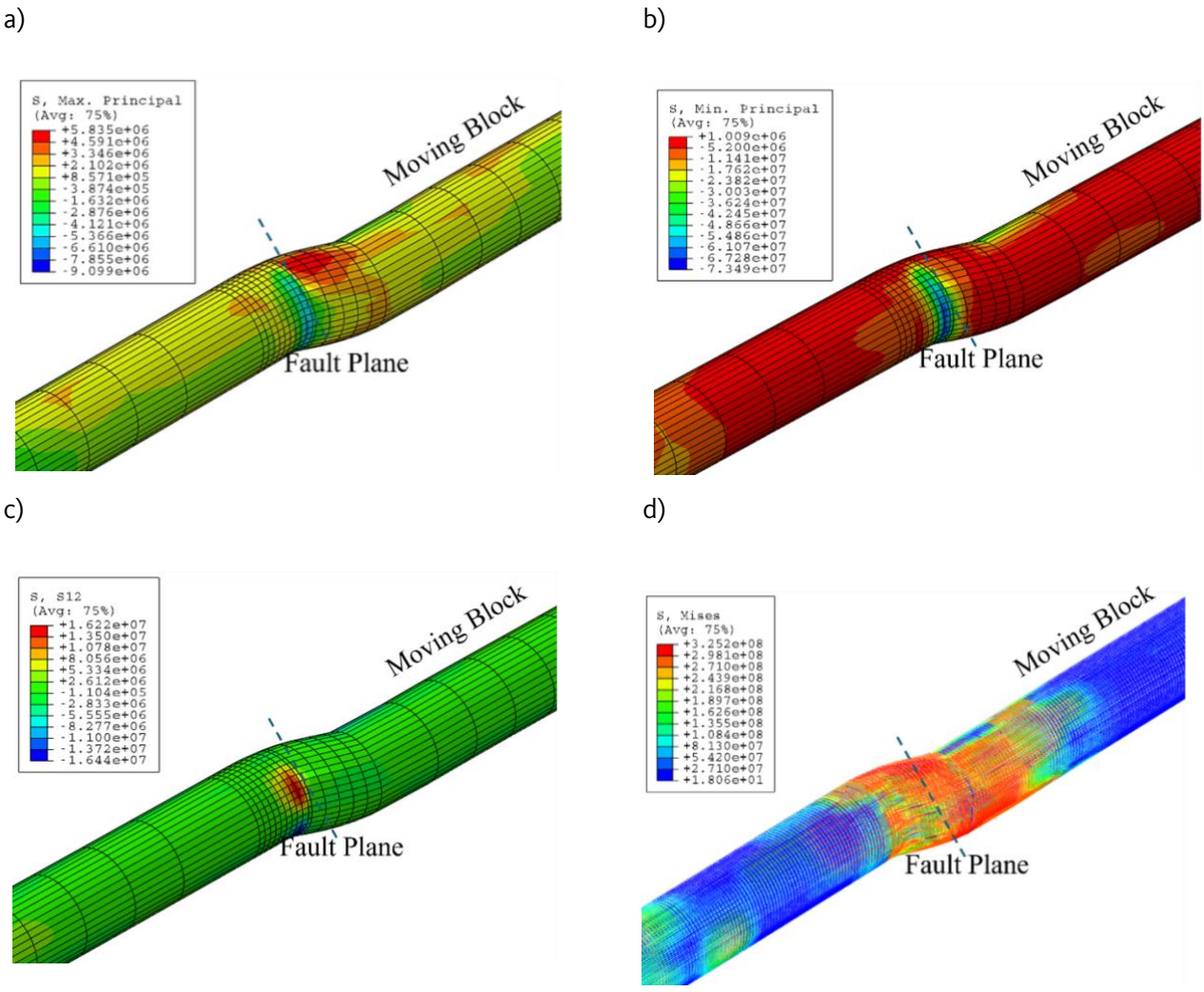

Figure 15. a) Maximum principal stress, b) Minimum principal stress, and c) Shear stress distributions of the tunnel lining, d) Von Misses stress distributions in the reinforcement steel bars for a fault displacement of 1.5 m (units in Pascal).

Influence of Rock Properties

To investigate the influence of rock properties on tunnel lining stresses, we analyzed the impact of the ratio of the elastic modulus at the fault zone (gouge) over that at the adjacent rock (serpentine). To investigate the fault zone's nonlinear behavior on lining stress, we varied fault zone cohesion (c) values.

Figure 16a illustrates the maximum Von Mises stresses at the crown, invert, and right and left walls of the tunnel for E_{gouge}/E_{serp} ratios of 0.3, 0.6, and 0.9. These ratios are less than unity because the fault zone material is damaged by faulting and therefore has a lower elastic modulus than the adjacent rock. The base (or original) model had an E_{gouge}/E_{serp} ratio of 0.3. The maximum stress increase was observed at the crown level with E_{gouge}/E_{serp}=0.9. While lining stresses increased with the E_{gouge}/E_{serp} ratio, the effect is small.

Figure 16b illustrates the impact of fault zone cohesion on lining stresses. We adjusted the cohesion from 0.5 MPa to 0.3 MPa and up to 1.5 MPa. Increasing cohesion generally reduced lining stresses, with a more significant effect observed at the right wall. We observed that lower cohesion values also caused stresses to shift further into the fault zone (on the fixed block side) from the fault plane. These results suggest that cohesion values have a more pronounced impact on lining stresses than elastic properties of the surrounding rock. Note that the extent of damage along the tunnel axis, as discussed in the following section, was assessed based on the base model parameters.

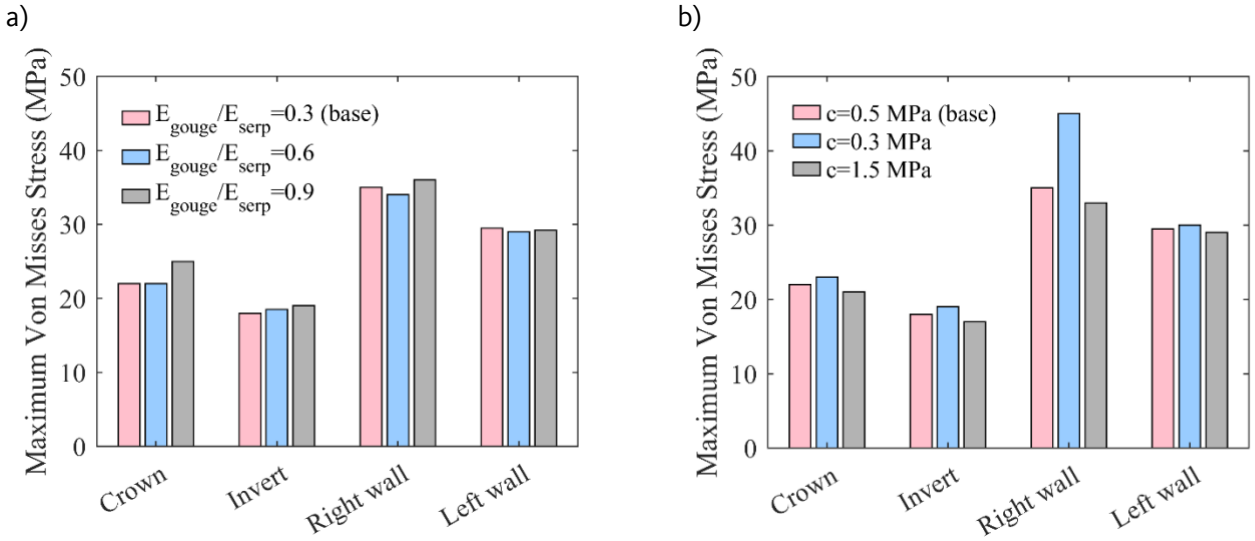

Figure 16. a) The maximum Von Mises stresses at the crown, invert, and right and left walls of the tunnel for various E_{gouge}/E_{serp} ratios b) The impact of fault zone cohesion on lining stresses.

Quantification of the Tunnel Damage

As shown in previous sections, strike-slip fault displacements cause the tunnel lining to experience complex combinations of axial, bending, and shear strains. To quantify the extent of damage in the lining, we computed the compression and tension damage parameters of the Concrete Damage Plasticity (CDP) material model. Figure 17 illustrates the changes in DAMAGEC and DAMAGET based on strain levels. Additionally, the shear strain capacity of the C20 concrete and steel bar yielding (i.e., 0.14 %) are represented by dashed lines.

The results in Figure 17 show that when DAMAGET < 0.7, no compression damage or steel yielding occurs but that the shear strain capacity is exceeded when DAMAGET > 0.4, which can lead to diagonal shear cracks. These results suggest that the lining may develop minor to moderate diagonal cracks when DAMAGET ranges from 0.4 to 0.7 (i.e., a further evolution of the diagonal cracking from fault creep as described in *Validation of the Numerical Model*), whereas for DAMAGET > 0.7, major cracks and spalling of concrete are likely. Concrete crushing occurs when DAMAGEC reaches 0.6, indicating that the concrete reaches its compressive strain limit (around 0.3%) and its capacity to support compressive loads is significantly reduced.

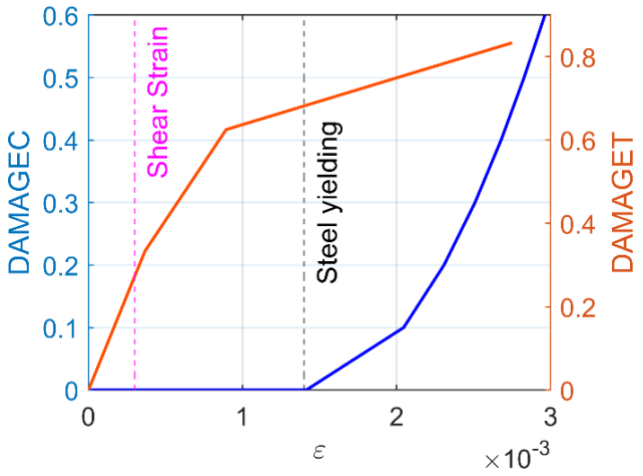

Figure 17. Strain vs. Compression/Tension damage, shear strain capacity of the C20, and the steel yielding strain.

Figure 18a-b illustrates the DAMAGET distributions at fault displacements of 0.04 m and 0.2 m, corresponding to the 10-year and 60-year creep displacements, respectively, where the former corresponds to the displacement level considered in the *Validation* section and the latter corresponds to the present-day creep displacement. As the creep displacement level increases, DAMAGET also increased, indicating that the severity of the cracks became more pronounced. From 0.04 m to 0.2 m, the tensile damage range in the Z-direction expanded from D_{outer} to $2D_{outer}$ in the moving block. The extent of damage in the moving block was higher than in the fault zone region. No compression damage was predicted at these displacement levels.

Information on actual damage to the tunnel lining at the present time is not available, so we are unable to confirm the predicted liner damage. However, we have indirect evidence of damage from BART Tunnels and Structures (2017), which planned to conduct creep repairs to the tunnel cross section for improved train operation. In 2019, DMZ Builders completed a surface treatment project in the Berkeley Hills Tunnel. This work included installing anchored wire mesh panels and epoxy injections to mitigate hazards to moving trains from fractures and loose concrete within the tunnel lining.

Figure 18c-d depicts DAMAGEC and DAMAGET distributions along the tunnel axis at a fault displacement of 1.5 m. Since the damage extended over a distance in the Z-direction of about 20-30 m, only ±15 m from the fault plane is shown in the figures. When δ = 1.5 m, DAMAGEC reached its maximum value, with the damage range in the Z-direction extending to $0.5D_{outer}$ within the fault zone on the fixed block side and to $1D_{outer}$ in the moving block. This indicates significant compression/ shear damage is expected in these areas, which is consistent with the longitudinal compressive strains and shear strain distributions observed at the crown and invert levels (Figures 12a-b, 14a-b). On the other hand, DAMAGET extended over greater lengths along the tunnel axis (in the Z-direction) compared to DAMAGEC. Tension damage was consistent with the curvature behavior of the tunnel: the right wall of the tunnel located in the moving block experienced tensile strains due to section bending, while the left wall in the fixed block side underwent tensile strains from section bending. Thus, the peak

DAMAGET was concentrated in these regions, within a distance of $2D_{outer}$ from the fault plane. The invert and crown regions also exhibited significant DAMAGET near the fault plane, approximately $1D_{outer}$ from the fault plane, due to high shear stress concentrations.

Steel yielding was observed in regions where DAMAGET > 0.7, typically occurring in the sidewalls of the tunnel where bending-induced tensile stresses were highest. As fault displacement increased, steel yielding was seen circumferentially within a distance of $3D_{outer}$ from the fault plane in the moving block and $1D_{outer}$ in the fault zone on the fixed block side (see Figure 15d).

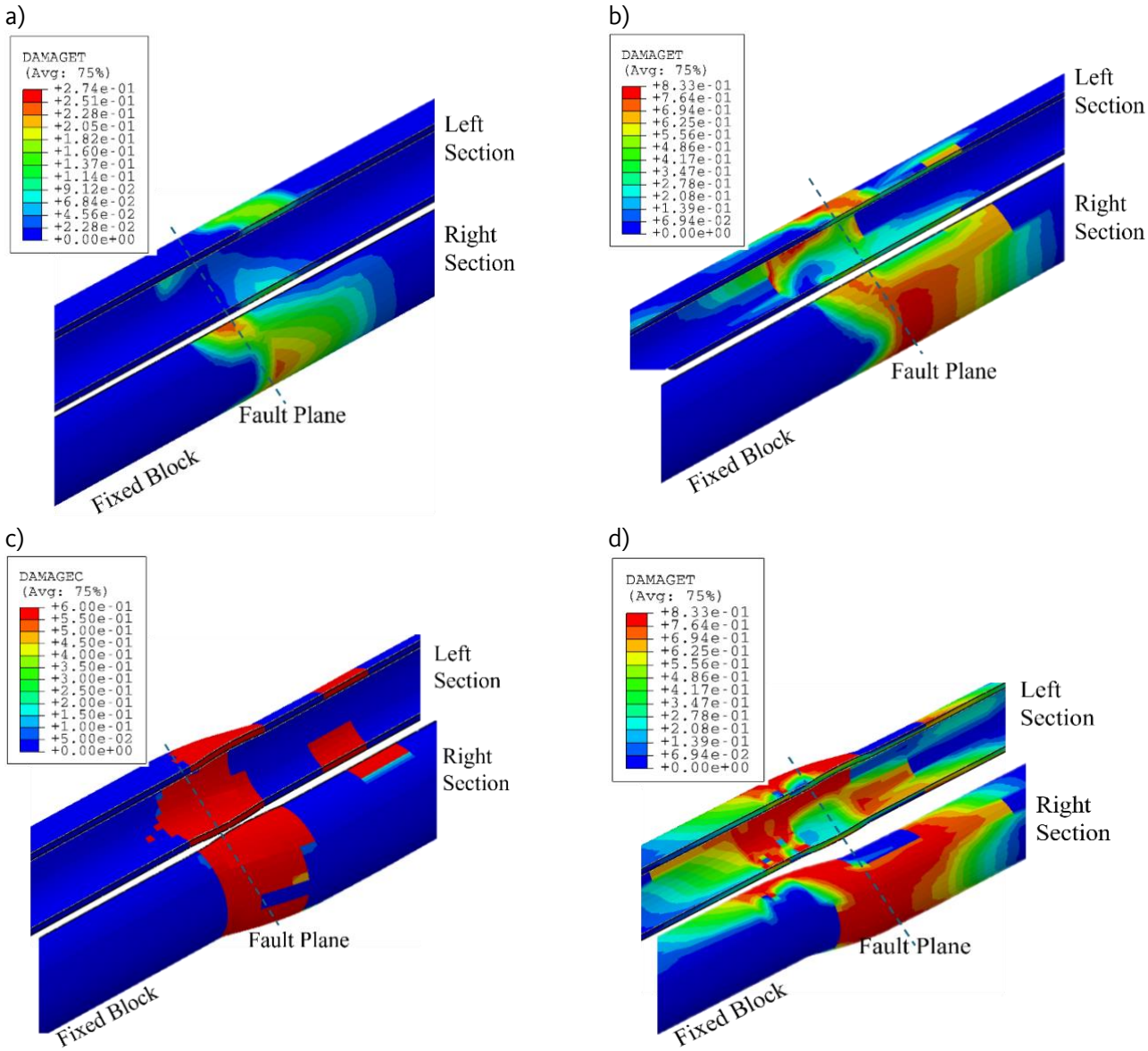

Figure 18. a) Concrete tension damage (DAMAGET) distributions along the tunnel axis at fault displacements of a) 0.04 m and b) 0.2 m, corresponding to the 10-year and 60-year creep displacements c)

Concrete compression damage (DAMAGEC) and d) DAMAGET distributions along the tunnel axis at a fault displacement of 1.5 m.

Functionality Impact and Restoration Timeline

Table 3 provides an overview of structural damage characteristics, functionality impacts, and restoration timelines for varying fault displacement levels, along with their associated return periods and exceedance probabilities over a 50-year lifespan. The return periods in this table are based on probabilistic fault displacement analyses using FDHI models as presented in Figure 10. “Functionality” refers to the type of repairs needed and the impact on the train operations. The restoration timeline reflects how quickly trains can resume full service. While the design speed for trains is 129 km/h (80 mph), repairs to the tunnel lining would require them to operate at a reduced speed of 56 km/h (35 mph). Our analysis focused on one bore of the Berkeley Hills Tunnel, but similar damage patterns are expected in the other bore due to the tunnel’s symmetrical structure. In this case, a partial closure of the tunnel would allow limited operation in one bore while the other is fully closed for repairs.

The Lifelines Restoration Performance Project (City and County of San Francisco 2020) established restoration timelines for the BART system under a San Andreas Fault scenario. The project estimated that repairs to heavily damaged, safety-retrofitted stations and rail lines would be completed within approximately six months, with full restoration of BART service expected within the same timeframe. For the Hayward Fault scenario, however, they indicated that repairs to the Berkeley Hills Tunnel may take six months to a year. Specific restoration timelines for the Hayward Fault scenario were not provided. They also pointed out that these projections should be interpreted as indicative of potential restoration challenges rather than predictive of actual performance following future seismic events. The "Functionality and Restoration Timeline" column in Table 3 provides an approximate estimate of restoration times, which are based on the authors’ engineering judgement regarding the impact of lining damage to train operations. These estimates have been validated as being reasonable through feedback from a BART engineer. During the progress of this project, we have had multiple fruitful technical discussions with BART and we have shared our methodology, assumptions and findings. A draft of this report has also been shared with BART. Our ongoing interactions with BART have been integral to this project.

At a displacement of 0.2 m, which corresponds to a return period of approximately 327 years, the tunnel experienced steel bar yielding and tension damage with major cracks extending up to 5 m along the sidewalls and minor cracks over 10 m along the tunnel length at the crown and invert levels. Diagonal cracks may also appear near the fault plane. Repairs may involve patching these affected areas, leading to minimal disruption and repair time of within 1 to 4 weeks. At 0.5 m displacement, with a return period of 384 years, diagonal shear cracks and partial concrete spalling over 3 m were observed, with major cracks extending over 15 m at the fault zone and moving block. In this case, repairs may become more complex, requiring surface treatment, localized concrete replacement, and crack sealing, which may necessitate temporary train speed restrictions or partial closures for approximately three months. At 1.0 m displacement, linked to a return period of 500 years, significant damage including concrete crushing, exposed reinforcement, and partial collapse over about 4 m of

tunnel length in the Z-direction would likely require full or partial tunnel closures. Extensive repairs may involve concrete replacement, additional reinforcements, potentially precast concrete segment reconstruction, and track realignment with a restoration period of around six months. At 1.5 m, with a return period of 654 years, severe shearing or partial collapse over 8 to 20 m of tunnel length may possibly demand a full tunnel closure and major service interruptions. The comprehensive reconstruction strategy may include large-scale reinforcement, complete lining replacement, and track realignment among other possible actions, with a restoration timeline possibly extending from 12 to 24 months. A 1000-year event corresponds to approximately 2.5 m of fault displacement. Since the damage characteristics in the tunnel lining for 1.5 m and higher would be similar, we did not show this case in detail. These findings emphasize the increasing complexity and extended timelines for structural repair, track realignment and train operations as fault displacements increase. This highlights the need for proactive repair strategies and timely interventions to manage disruptions and ensure the safety and functionality of the tunnels.

Table 3. Structural Damage Characteristics, Functionality Impact, and Restoration Timelines for Tunnel Lining at Various Fault Displacement Levels, Along with Associated Return Periods and Exceedance Probabilities.

Fault displacement (m)	Return period (years)	Exceedance probability over a 50-year tunnel lifespan	Description of the damage	Functionality & Restoration timeline
0.2	327	14%	Steel bars yielding at the tension zone. Major cracks in tunnel lining at the tunnel side walls over 5 m and minor cracks over 10 m length at the crown/invert levels located near fault plane and moving block. Diagonal cracks may be observed near fault plane.	Structural repairs involve patching the affected areas. Minimal disruption to train operations; realignment and repairs may be completed within 1-4 weeks.
0.5	384	12%	Diagonal shear cracks near the fault plane, partial concrete spalling over 3 m at the crown/ invert levels. Major cracks distributed over 15 m in the tunnel lining at the fault zone and moving block.	Structural repairs include surface repair, localized concrete replacement, and crack sealing. Temporary speed restrictions or partial closures may be necessary (approximately 3 months).

Fault displacement (m)	Return period (years)	Exceedance probability over a 50-year tunnel lifespan	Description of the damage	Functionality & Restoration timeline
1.0	500	9.5%	Significant damage to the lining, crushing of concrete, exposed reinforcement, loss of stability and partial collapse over a span of 4 m.	Full or partial tunnel closures likely; considerable disruptions to train operations with complex repair strategies including concrete replacement, installation of additional reinforcements, and possibly precast concrete segment reconstruction (approximately 6 months).
1.5	654	7%	The lining may shear off, partial collapse over a span of 8 to 20 m.	Full tunnel closure expected, major service interruptions with detailed planning for repair execution and alternative routing. Reconstruction strategies involve large-scale reinforcement, complete lining replacement, among other possible actions (12-24 months).

Conclusions

This study provides insights into how the Berkeley Hills Tunnel crossing the Hayward Fault would respond to varying fault displacements. The findings revealed that fault displacements could induce substantial strains and stresses in the tunnel lining, with the severity of the damage increasing with the amount of displacement. By analyzing longitudinal and shear strains, along with curvature behaviors at critical tunnel locations, such as the crown, invert, and sidewalls, we quantified the resulting compression and tension damage using the ABAQUS software. The results indicated that a fault displacement of 0.2 m led to significant tensile cracks extending up to 5 m along the length of the tunnel, while fault displacements of 1.0 m or more could lead to concrete crushing and severe structural damage, particularly near the fault plane. Our sensitivity analyses of lining stresses to rock properties showed that fault zone cohesion had a more pronounced impact on stresses than the elastic modulus ratio between the fault zone and adjacent rock, with lower cohesion values increasing stresses.

Increasing fault displacements may impact the functionality of the tunnel and restoration timelines. At 0.2 m, repairs may typically be completed approximately within one to four weeks with minimal operational disruption. At 0.5 m, repairs may take around three months and could involve partial closures or train speed restrictions. Fault displacements of 1.0 m may require up to approximately six months for extensive repairs, while a displacement of 1.5 m could lead to full tunnel closures with repair times extending from 12 to 24 months. These findings can guide strategies for enhancing short-term response plans and inform long-term recovery efforts, as they will be integrated into multimodal simulations to optimize post-earthquake transportation recovery (Soga et al. 2024).

Using the probabilistic fault displacement hazard analysis derived from the latest FDHI models, we determined that a fault displacement of 1.0 m was associated with a return period of 500 years, which had a 9.5 percent probability of being exceeded within a 50-year tunnel operating period. Such a displacement would likely cause significant damage to the tunnel, potentially leading to partial or complete closure. The results suggest that the tunnel did not achieve BART system's long-term performance goal of remaining operational during a 500-year seismic event. Additionally, while 0.2 m displacement has a return period of 327 years, the creep of the Hayward Fault could cause such a displacement within the next 50 years. This highlights the necessity for ongoing monitoring and proactive measures to mitigate damage and operational disruptions.

The Local Hazard Mitigation Plan (2017) proposed designing a bypass for the Berkeley Hills Tunnel as a mitigation strategy, suggesting the creation of an alternate route around a vulnerable section of the tunnel. However, this action was assigned a lower priority compared to other initiatives in the 2022 update of the plan (Local Hazard Mitigation Plan 2022). Another potential mitigation strategy may involve retrofitting the existing tunnel by adjusting its geometry to facilitate more rapid post-event repair. This retrofit could involve enlarging the tunnel dimensions in the horizontal direction (to facilitate re-alignment post-event) and increasing the liner thickness (to reduce liner damage from fault displacement). However, this study did not evaluate how such

modifications would impact tunnel performance under fault displacement. Thus, further studies are needed to examine the feasibility and effectiveness of these retrofits.

In this study, we characterized compression and tension damage based on unconfined concrete behavior, which potentially led to conservative damage predictions. Steel reinforcement could improve the strength and ductility of the concrete, which may reduce the severity of the damage. Future research should also integrate seismic shaking and fault displacement to assess their combined impact on tunnel damage.

References

Allam, Said M., Mohie S. Shoukry, Gehad E. Rashad, and Amal S. Hassan. 2013. "Evaluation of tension stiffening effect on the crack width calculation of flexural RC members." *Alexandria Engineering Journal*, 52, no. 2: 163-173.

American Concrete Institute (ACI 318-19). 2019. *Building code requirements for structural concrete and commentary*, Farmington Hills, MI.

Anastasopoulos, Ioannis, Nikos Gerolymos, Vasileios Drosos, Takis Georgarakos, Rallis Kourkoulis, and George Gazetas. 2008. "Behaviour of deep immersed tunnel under combined normal fault rupture deformation and subsequent seismic shaking," *Bulletin of Earthquake Engineering*, 6: 213-239.

Asakura, Toshihiro, and Yutaka Sato. 1998. "Mountain tunnels damage in the 1995 Hyogoken-Nanbu earthquake," *Quarterly Report-RTRI*, 39: 9-16.

Ayres, M.O. 1969. "Case history - Berkeley Hills twin transit tunnels," *Proceedings of the Second Symposium on Rapid Excavation, Sacramento CA*. Sacramento State College.

BART Tunnels and Structures. 2017. "Repair tunnels & structures –$570 Million" https://www.bart.gov/sites/default/files/better-bart/repair%20tunnels%20structures.pdf. Accessed September 20, 2024.

Bay Area Rapid Transit (BART). 2024a. "BART Facts 2024." https://www.bart.gov/sites/default/files/2024-01/BARTFacts2024.pdf. Accessed September 20, 2024.

BART. 2024b. "Earthquake Safety Program Technical Information." https://www.bart.gov/about/projects/eqs/technical. Accessed September 20, 2024.

Bechtel. 1968. *Completion report of the construction engineering geology of the Berkeley Hills tunnel, Central Contra Costa Line*. Unpublished Report.

Bechtel. 1970. *BART Berkeley Hills tunnels, Hayward Fault zone instrumentation*. Unpublished Report.

Bechtel. 2000. "BART Seismic Vulnerability Study." https://www.bart.gov/sites/default/files/docs/50-years/2000%20BART%20Seismic%20Vulnerability%20Study.pdf. Accessed September 20, 2024.

Blake Jr., M. Clark, David G. Howell, and Angela S. Jayko. 1984. "Tectonostratigraphic terranes of the San Francisco Bay region," In *Franciscan Geology of Northern California, Vol. 43*, edited by M. Clark Blake Jr., pp. 5-22 Pacific Section, Society of Economic Paleontologists and Mineralogists (SEPM).

Brown, Ian R., Tor L. Brekke, and Gregory E. Korbin. 1981. *Behavior of the Bay Area Rapid Transit tunnels through the Hayward fault*, No. UMTA-CA-06-0120-81-1, U.S. Department of Transportation, Urban Mass Transportation Administration.

Burridge, Paul B., Ronald F. Scott, and John F. Hall. 1989. "Centrifuge study of faulting effects on tunnel," *Journal of Geotechnical Engineering*, 115, no. 7: 949-967.

Bürgmann, Roland, Eric Fielding, and Jai Sukhatme. 1998. "Slip along the Hayward fault, California, estimated from space-based synthetic aperture radar interferometry," *Geology* 26, no. 6: 559-562.

California Geological Survey. 2006. "Earthquakes of the San Francisco Bay Area and Northern California," *California Geology*, Special Edition. https://www.conservation.ca.gov/cgs/Documents/Publications/Special-Publications/SP_125.pdf. Accessed September 20, 2024.

City and County of San Francisco. 2020. "Lifelines Restoration Performance Project." https://www.onesanfrancisco.org/sites/default/files/inline-files/Lifelines%20Restoration%20Performance%20Report%20Final.pdf. Accessed September 20, 2024.

Corigliano, Mirko, Laura Scandella, Carlo G. Lai, and Roberto Paolucci. 2011. "Seismic analysis of deep tunnels in near fault conditions: a case study in Southern Italy," *Bulletin of Earthquake Engineering*, 9: 975-995.

Dassault Systèmes Simulia Corp. 2020. *Abaqus analysis user's guide*. https://www.3ds.com/support/documentation/user-guides. Accessed September 20, 2024.

Dassault Systèmes Simulia Corp. 2013. *ABAQUS Documentation, Theory Manual*.

Detweiler, Shane T. and Anne M. Wein, eds. 2017. *The HayWired Earthquake Scenario—Earthquake Hazards*. U.S. Geological Survey, Scientific Investigations Report 2017–5013–A–H. DOI: 10.3133/sir20175013v1

DMZ Builders. 2019. "Berkeley Hills Tunnels Lining Surface Treatment." https://www.dmzbuilders.com/project/berkeley-hills-tunnels-lining-surface-treatment/

Field, Edward H., Glenn P. Biasi, Peter Bird, Timothy E. Dawson, Karen R. Felzer, David D. Jackson, Kaj M. Johnson, et al. 2015. "Long-term time-dependent probabilities for the third Uniform California Earthquake Rupture Forecast (UCERF3)," *Bulletin of the Seismological Society of America*, 105, no. 2A: 511-543.

Gao, Jiaqing, Qiyao Wang, Weigang Ma, and Junzhang Lu. 2024. "Failure analysis and comparative study on tunnels under strike-slip fault and oblique-slip fault movements," *Engineering Failure Analysis*, 164: 108676.

Geomatrix Consultants. 2001. *Fault rupture hazard evaluation, California Memorial Stadium*, Report prepared for Capitol Projects, University of California, Berkeley, October.

Hashash, Youssef MA, Jeffrey J. Hook, Birger Schmidt, I. John, and Chiang Yao. 2001. "Seismic design and analysis of underground structures," *Tunnelling and Underground Space Technology*, 16, no. 4: 247-293.

Hudnut, Kenneth W., Anne M. Wein, Dale A. Cox, Keith A. Porter, Laurie A. Johnson, Suzanne C. Perry, Jennifer L. Bruce, Drew LaPointe. 2018. "*The HayWired earthquake scenario—We can outsmart disaster*," *U.S. Geological Survey Fact Sheet 2018–3016*. https://doi.org/10.3133/fs20183016

Iida, Hiroomi, Toshio Hiroto, Nozomu Yoshida, and Masahiko Iwafuji. 1996. "Damage to Daikai subway station," *Soils and Foundations*, 36: 283-300.

Kennedy, Robert P., Robert A. Williamson, and Andrew M. Chow. 1977. "Fault movement effects on buried oil pipeline," *Transportation Engineering Journal of ASCE*, 103, no. 5: 617-633.

Kent, Dudley Charles, and Robert Park. 1971. "Flexural members with confined concrete," *Journal of the Structural Division* 97, no. 7: 1969-1990.

Kiani, Majid, Abbas Ghalandarzadeh, Tohid Akhlaghi, and Mohammad Ahmadi. 2016. "Experimental evaluation of vulnerability for urban segmental tunnels subjected to normal surface faulting," *Soil Dynamics and Earthquake Engineering*, 89: 28-37.

Kuehn, Nicolas M, Albert Kottke, Alexandra Sarmiento, Danielle Madugo and Yousef Bozorgnia. 2024. "A fault displacement model based on the FDHI database," *Earthquake Spectra*, in press.

Lai, Jinxing, Siyue He, Junling Qiu, Jianxun Chen, Lixin Wang, Ke Wang, and Junbao Wang. 2017. "Characteristics of seismic disasters and aseismic measures of tunnels in Wenchuan earthquake," *Environmental Earth Sciences*, 76: 1-19.

Lanzano, Giovanni, Emilio Bilotta, Gianpiero Russo. 2008. "Tunnels under seismic loading: a review of damage case histories and protection methods," In *Strategies for Reduction of the Seismic Risk*, edited by Giovanni Fabbrocino and Filippo Santucci de Magistris, pp. 65-74. ISBN 88-88102-15-3

Laursen Tod A. 2002. Computational Contact and Impact Mechanics. Springer, Berlin.

Lavrentiadis, Grigorios, Norman Abrahamson. 2023. "Fault-displacement models for aggregate and principal displacements," *Earthquake Spectra*, DOI: 87552930231201531

Leone, Thomas, Alexandros N. Nordas, and Georgios Anagnostou. 2024. "Effects of creep on shield tunnelling through squeezing ground," *Rock Mechanics and Rock Engineering*, 57, no. 1: 351-374.

Lienkaemper, James J., and Jon Scott Galehouse. 1997. "Revised long-term creep rates on the Hayward fault, Alameda and Contra Costa counties, California," *U.S. Department of the Interior*, U.S. Geological Survey.

Lienkaemper, James J., Jon S. Galehouse, and Robert W. Simpson. 1997. "Creep response of the Hayward fault to stress changes caused by the Loma Prieta earthquake," *Science* 276, no. 5321: 2014-2016.

Local Hazard Mitigation Plan. 2017. “BART Local Hazard Mitigation Plan.” https://www.bart.gov/sites/default/files/docs/Final%20Local%20Hazard%20Mitigation%20Plan_06022017.pdf

Local Hazard Mitigation Plan. 2022. “BART Local Hazard Mitigation Plan.” https://www.bart.gov/sites/default/files/docs/Local%20Hazard%20Mitigation%20Plan__2022-06-02.pdf

Lubliner, Jacob, Javier Oliver, Sand Oller, and Eugenio Onate. 1989. “A plastic-damage model for concrete,” *International Journal of Solids and Structures* 25, no. 3: 299-326.

Luo, Xingwen, and Zhenjun Yang. 2013. “Finite element modeling of a tunnel affected by dislocation of faults,” *Proceedings of 5th Asia Pacific Congress on Computational Mechanics and 4th International Symposium on Computational Mechanics (APCOM & ISCM)*, Singapore. https://www.sci-en-tech.com/apcom2013/APCOM2013-Proceedings/PDF_FullPaper/1329.pdf

Ma, Yalina, Qian Sheng, Guimin Zhang, and Zhen Cui. 2019. “A 3D discrete-continuum coupling approach for investigating the deformation and failure mechanism of tunnels across an active fault: a case study of Xianglushan tunnel,” *Applied Sciences*, 9, no. 11: 2318.

McGarr, A., and Joe B. Fletcher. 2003. "Maximum slip in earthquake fault zones, apparent stress, and stick-slip friction," *Bulletin of the Seismological Society of America*, 93, no. 6: 2355-2362. DOI: 10.1785/0120030037.

Moss, Robb Eric S., and Zachary E. Ross. 2011. “Probabilistic fault displacement hazard analysis for reverse faults,” *Bulletin of the Seismological Society of America*, 101 no. 4: 1542-1553.

Newmark, Nathan Mortimore. 1975. “Pipeline design to resist large fault displacement,” *Proceedings of U.S. National Conference on Earthquake Engineering*, 416-425.

Owen, G. Norman, and Roger E. Scholl. 1981. “Earthquake engineering of large underground structures,” prepared for the Federal Highway Administration, FHWAIRD-801195.

Petersen, Mark D., Timothy E. Dawson, Rui Chen, Tianqing Cao, Christopher J. Wills, David P. Schwartz, and Arthur D. Frankel. 2011. “Fault displacement hazard for strike-slip faults,” *Bulletin of the Seismological Society of America*, 101, no. 2: 805–825.

Pitilakis, K., G. Tsinidis. 2013. “Performance and seismic design of underground structures,” In *Earthquake Geotechnical Engineering Design*, edited by Michele Maugeri and Claudio Soccodato, pp. 279-340. Cham: Springer International Publishing.

Russo, M., G. Germani, and W. Amberg. 2002. “Design and construction of large tunnel through active faults: a recent application,” *Proceedings International Conference of Tunneling and Underground Space Use,* Istanbul, pp. 1-14.

Sarmiento, Alexandra, Danielle Madugo, Andi Shen, Timothy Dawson, Chris Madugo, Stephen Thompson, Yousef Bozorgnia, et al. 2024a. "Database for the Fault Displacement hazard initiative project," *Earthquake Spectra*, 87552930241262766.

Sarmiento, Alexandra, Grigorios Lavrentiadis, Yousef Bozorgnia, Rui Chen, Brian S. J. Chiou, Timothy E. Dawson, Albert Kottke, et al. 2024b. "Comparisons of FDHI fault displacement models for aggregate and principal displacements," *Earthquake Spectra*, in Press.

Shi, S. 1999. "Shear strength, modulus of rigidity and young's modulus of concrete," *China Civil Engineering Journal*, 32: 47–52. (In Chinese)

Soga, Kenichi, Louise Comfort, Bingyu Zhao, Yili Tang, Tianyu Han. 2024. "Assessing the Functionality of Transit and Shared Mobility Systems after Earthquakes," Institute of Transportation Studies, University of California, Report No.: UC-ITS-RIMI-4KK, DOI: 10.7922/G2NZ860C.

Stirling, Mark, Tatiana Goded, Kelvin Berryman, and Nicola Litchfield. 2013. "Selection of earthquake scaling relationships for seismic-hazard analysis," *Bulletin of the Seismological Society of America*, 103, no. 6: 2993-3011.

Tao, Lianjin, Zhigang Wang, Cheng Shi, and Haixiang Zhang. 2023. "Investigation of the longitudinal mechanical response of pipeline or tunnel under reverse fault dislocation," *Rock Mechanics and Rock Engineering*, 56, no. 9: 6237-6259.

Thatcher, Wayne, Grant Marshall, and Michael Lisowski. 1997. "Resolution of fault slip along the 470-km-long rupture of the great 1906 San Francisco earthquake and its implications," *Journal of Geophysical Research: Solid Earth*, 102, no. B3: 5353-5367.

Tsinidis, Grigorios, Kyriazis Pitilakis, Gopal Madabhushi, and Charles Heron. 2015. "Dynamic response of flexible square tunnels: centrifuge testing and validation of existing design methodologies," *Geotechnique* 65, no. 5: 401-417.

Uenishi, Koji, and Shunsuke Sakurai. 2000. "Characteristic of the vertical seismic waves associated with the 1995 Hyogo-ken Nanbu (Kobe), Japan earthquake estimated from the failure of the Daikai Underground Station," *Earthquake Engineering and Structural Dynamics*, 29, no. 6: 813-821.

Ulusay, Resat, Ömer Aydan, and Masanori Hamada. 2002. "The behaviour of structures built on active fault zones: Examples from the recent earthquakes of Turkey," *Structural Engineering/Earthquake Engineering*, 19, no. 2: 149-167.

Wang, Wen-Li, Tai-Tien Wang, JJ Su, CH Lin, CR Seng, and TH Huang. 2001. "Assessment of damage in mountain tunnels due to the Taiwan Chi-Chi Earthquake," *Tunnelling and Underground Space Technology*, Volume 16, no. 3: 133-150.

Wang, Huanzi, Shirley Ng, Ahmad M. Abdel-Karim, Dan Weston. 2013. “Seismic Retrofit of Aerial Stations: Bay Area Rapid Transit, San Francisco, California,” *Transportation research record*, 2332: 3-12.

Wang, Tianqiang, and Ping Geng. 2024. “Quantitative damage evaluation of tunnel subjected to a subsequent strong seismic after a quasi-static reverse faulting,” *Engineering Failure Analysis*, 157, no. 2:107886.

Wells, Donald L., and Kevin J. Coppersmith. 1994. “New empirical relationships among magnitude, rupture length, rupture width, rupture area, and surface displacement,” *Bulletin of the Seismological Society of America*, 84, no. 4: 974-1002.

Yan, Gaoming, Boming Zhao, Zijun Wang, and Bo Gao. 2022. “Simplified analytical solution for responses of fault-crossing tunnels with flexible joints under fault movement,” *Structures*, 45:984-998.

Youngs, Robert R., Walter J. Arabasz, R. Ernest Anderson, Alan R. Ramelli, Jon P. Ake, David B. Slemmons, James P. McCalpin, et al. 2003. “A methodology for probabilistic fault displacement hazard analysis (PFDHA),” *Earthquake Spectra* 19, no. 1: 191-219.

Yu, Haitao, Juntao Chen, Yong Yuan, and Xu Zhao. 2016. “Seismic damage of mountain tunnels during the 5.12 Wenchuan earthquake,” *Journal of Mountain Science*, 13: 1958-1972.

Zhang, LF., RH Li, H Liu, ZB Fang, HB Wang, Yong Yuan, Haitao Yu. 2020. “A review on seismic response and aseismic measures of fault-crossing tunnels,” *IOP Conference Series: Earth and Environmental Science*, 570, no. 5: 052046. IOP Publishing.

Zhang, Xiao, Li Yu, Mingnian Wang, and Henghong Yang. 2024. “A mechanical analysis model for tunnels under strike-slip faulting considering the fault zone width and nonlinear tunnel-stratum interaction,” *Transportation Geotechnics*, 44, no. 1: 101171

Zhao, Chenyang, Arash Alimardani Lavasan, Thomas Barciaga, Christoph Kämper, Peter Mark, and Tom Schanz. 2017. “Prediction of tunnel lining forces and deformations using analytical and numerical solutions,” *Tunnelling and Underground Space Technology*, 64: 164-176.

Zhen, Cui, Sheng Qian, Zhang Gui-min, Zhang Mao-chu, and Mei Xian-cheng. 2022. “Response and mechanism of a tunnel subjected to combined fault rupture deformation and subsequent seismic excitation,” *Transportation Geotechnics*, 34, no. 8: 100749.